JOURNAL OF PROTEOMICS 85 (2013) 109–128

Available online at www.sciencedirect.com

SciVerse ScienceDirect

www.elsevier.com/locate/jprot

Original article

# Comparative proteome analysis of lung tissue from patients with idiopathic pulmonary fibrosis (IPF), non-specific interstitial pneumonia (NSIP) and organ donors

*Martina Korfei*[a], *Daniel von der Beck*[a], *Ingrid Henneke*[a], *Philipp Markart*[a,g], *Clemens Ruppert*[a], *Poornima Mahavadi*[a], *Bahil Ghanim*[b], *Walter Klepetko*[b,h], *Ludger Fink*[a,g], *Silke Meiners*[c,g], *Oliver Holger Krämer*[d], *Werner Seeger*[a,g], *Carlo Vancheri*[e,h], *Andreas Guenther*[a,f,g,h,*]

[a]*Universities of Giessen and Marburg Lung Center (UGMLC), D-35392 Giessen, Germany*
[b]*Department of Thoracic Surgery, Vienna General Hospital, A-1090 Vienna, Austria*
[c]*CPC-Comprehensive Pneumology Center Großhadern, D-81377 Munich, Germany*
[d]*Institute of Toxicology, Medical Center of the University Mainz, D-55131 Mainz, Germany*
[e]*Department of Clinical and Molecular Biomedicine, University of Catania, I-95123 Catania, Italy*
[f]*Agaplesion Lung Clinic Waldhof Elgershausen, D-35753 Greifenstein, Germany*
[g]*German Center for Lung Research, Germany*
[h]*European IPF Network and European IPF Registry, Germany*

## ARTICLE INFO

*Article history:*
Received 4 February 2013
Accepted 26 April 2013
Available online 6 May 2013

*Keywords:*
Idiopathic pulmonary fibrosis (IPF)
Non-specific interstitial pneumonia (NSIP)
DIGE technique
Type-II alveolar epithelial cell (AECII)
Oxidative stress
Antioxidant

## ABSTRACT

Among the idiopathic interstitial pneumonias (IIP), the two entities IPF and NSIP seem to be clinically related, but NSIP has a better outcome. The proteomic signatures which distinguish NSIP from IPF remain still elusive. We therefore performed comparative proteomic analysis of peripheral lung tissue from patients with sporadic IPF (n = 14) and fibrotic NSIP (fNSIP, n = 8) and organ donors (Controls, n = 10), by using the 2-dimensional DIGE technique and MALDI-TOF-MS. The study revealed that the proteomic profiles of IPF and fNSIP were quite similar. Among the upregulated proteins in IPF and fNSIP were stress-induced genes involved in the ER stress-pathway, whereas downregulated proteins in IPF and fNSIP included antiapoptotic factors and antifibrotic molecules. The comparison fNSIP versus IPF indicated upregulation of subunits of the proteasome activator complex and antioxidant enzymes of the peroxiredoxin family. We conclude, that only few protein expression changes exist between IPF and fNSIP, and that epithelial ER- and oxidative stress play a major role in the pathogenesis of both diseases. In contrast to IPF, intracellular clearance of ROS and misfolded protein carbonyls seem to be enhanced in fNSIP due to enhanced expression of antioxidant acting proteins, and may explain the better outcome and survival in patients with fNSIP.

* *Corresponding author at:* Universities of Giessen and Marburg Lung Center (UGMLC), Department of Internal Medicine II, Klinikstrasse 36, 35392 Giessen, Germany. Tel.: +49 641 99 42515; fax: +49 641 99 42508.
E-mail address: Andreas.Guenther@innere.med.uni-giessen.de (A. Guenther).


http://dx.doi.org/10.1016/j.jprot.2013.04.033

Biological significance
IPF and fibrotic NSIP (fNSIP) belong to the idiopathic interstitial pneumonias and are usually fatal, but fNSIP has a better outcome. In order to identify molecular mechanisms and differences between IPF and fNSIP, we herein present results of a comparative proteome analysis of IPF, fNSIP and control lung tissue. Our data including validation experiments suggest that ER stress and a general stress-response as well as the decline of antioxidant capacity in alveolar epithelium is key in the pathogenesis of IPF and fNSIP. In addition, we could observe a signature of an increased alveolar epithelial protection against oxidative and ER-stress in fNSIP as compared to IPF, which could help to explain the better outcome of fNSIP patients.



## 1. Introduction

The idiopathic interstitial pneumonias (IIPs) are a heterogenous group of diffuse parenchymal lung diseases of unknown etiology, which are characterized by distortion of distal lung architecture by variable inflammation and fibrosis [1]. Of the IIPs, idiopathic pulmonary fibrosis (IPF) and nonspecific interstitial pneumonia (NSIP) have provoked most attention and also debate. Although IPF and NSIP can present in a clinically similar manner, it is currently accepted that they are different diseases, especially with respect to prognosis [1,2]. IPF, histologically defined by the usual interstitial pneumonia (UIP) pattern, is a disease in individuals aged 50 to 60 years and occurs somewhat more frequently in men [3–5]. UIP is characterized by dense fibrosis that causes destruction of the alveolar architecture with frequent honeycombing and bronchiolization of the alveoli, scattered fibroblast foci, and patchy lung involvement. At low magnification, the lung characteristically has a heterogenous appearance with alternating areas of normal parenchyma, fibrosis, and (bronchiolized) honeycomb cysts [1,3,4].

NSIP patients tend to be approximatively 10 years younger than IPF subjects, are more frequently female and may be sub-differentiated into cellular (cNSIP) and fibrotic NSIP (fNSIP) [1,2,5–7]. The histology of NSIP is temporally uniform, without the spatial and temporal heterogeneity of UIP. When NSIP is predominantly cellular, chronic interstitial inflammation involves the alveolar walls. In fNSIP, fibrosis consists of uniform collagen accumulation, resulting in expansion of alveolar septa and peribronchiolar interstitium without the patchwork distribution of UIP. Honeycombing and fibroblastic foci are rare [2,5].

Regarding prognosis, the average survival time in IPF from time of diagnosis is 2–3 years, due to the quite aggressive course of this disease [1,3,4]. In marked contrast, cNSIP appears as a rather benign disease with slow progression. Patients with cNSIP usually show a good response to steroid treatment, and an only modest limitation in life expecting [8,9]. The prognosis of patients with fNSIP seems to be in between IPF and cNSIP [5]. It has also been suggested that IPF/UIP simply represents a late presentation stage of untreated (or poorly responsive) NSIP [10,11]. With regard to therapy, pirfenidone has been authorized for treatment of mild to moderate IPF only [12], and steroid/immunosuppressive therapy has recently found to be inefficient in this disease [13]. In contrast, steroids/immunosuppressants seem to work in cNSIP, but not in fNSIP [8].

In summary, despite the prognostic and therapeutic implications, it is often clinically difficult to distinguish IPF from fNSIP, and, in absence of a definite UIP pattern in HRCT, surgical lung biopsy is still considered as diagnostic gold standard for both disorders [1–4]. Therefore, there is a great need for surrogates for diagnosis of both fatal diseases.

The molecular pathomechanisms underlying IPF and NSIP are incompletely understood, with most studies being done in the field of IPF. According to these, IPF is thought to be the result of a chronic injury to the alveolar epithelium, with continueous activation of aberrant repair processes and consecutive replacement of alveolar architecture by fibrotic scars and cysts lined by abnormal bronchiolar epithelium [14–17]. In line with this, apoptosis of type-II alveolar epithelial cells (AECII) is a prominent finding in IPF [18–22], but has also been observed in patients with exogen allergic alveolitis (EAA), cNSIP and fNSIP [23,24]. Such observation is supported by the finding of SP-C gene mutations in familial forms of IIP (mostly IPF and NSIP), which have been shown to result in the production of abundant misfolded proproteins, causing proteasome inhibition and endoplasmic reticulum (ER) stress, and finally, death of the AECII [25–27]. Moreover, proapoptotic ER stress in AECII is also a prominent feature in patients with sporadic IPF in the absence of any gene mutation [28]—and does not seem to differ in extent from familial IPF cases [29]. With regard to NSIP, however, data are much more scarce. According to our own preliminary studies, the extent of the proapoptotic ER stress response in AECII may almost be identical in fibrotic NSIP as compared to IPF [30]. However, the precise trigger mechanisms that culminate in ER stress, and AECII cell death are still unknown and molecular signatures and pathways that distinguish (fibrotic) NSIP from UIP remain elusive. To this end, comparative gene expression profiling in patients with UIP and NSIP (both: cNSIP and fNSIP) showed that there are consistent, but only few significant differences between the two types of IIP at the transcriptional level [10,11,31]. However, the lung proteomic patterns of the different types of IIP have yet not received attention. We hypothesized that IPF and fNSIP may exhibit different proteome signatures that may be useful to distinguish both entities, hence allowing development of new, disease-specific biomarkers and detection of molecular pathomechanisms/signatures that underlie the distinct lung phenotypes in IPF and fNSIP. We therefore performed a comparative proteome analysis of subpleural lung tissue from patients with sporadic IPF and fNSIP, with explanted donor lungs serving as controls. We employed the 2-Dimensional Difference in Gel Electrophoresis (2D-DIGE) approach, which allows the simultaneous co-separation of multiple, fluorescently labelled

samples on a single 2D-gel, thus representing an effective way to remove gel-to-gel variation, thereby significantly increasing accuracy and reproducibility. The present study reports the separation and comparison of the IPF-, fNSIP- and healthy control lung proteome on one and the same 2D-gel, and reports the validation and cellular localization of specifc proteomic signatures in all categories. To our surprise, the proteomic profiles of IPF and fNSIP were quite similar and only differed with regard to subunits of the proteasome activator complex and antioxidant enzymes, and cytokeratin-19.

## 2. Material and methods

### 2.1. Human lung tissue

Lung tissue samples were obtained from 14 patients with IPF (UIP pattern; mean age ± SD: 54.29 ± 14.40 years; 4 females, 10 males), 8 patients with fibrotic NSIP (fNSIP; mean age ± SD: 51.25 ± 8.52 years; 5 females, 3 males), and 10 control subjects (organ donors; mean age ± SD: 46.20 ± 18.25 years; 5 females, 5 males). Explanted lungs or lobes were obtained from the Dept. of Thoracic Surgery, Vienna (W. Klepetko). Already at the surgical theatre, peripheral lung tissue samples were snap-frozen or placed in 4% (w/v) paraformaldehyde immediately after explantation. Thereafter, the remaining lung lobes were placed on ice, and shipped (together with the other samples) to our institute immediately. Upon arrival, lung lobes were sectioned under the hood on ice according to a predefined algorithm; and additional lung tissue samples from subpleural and hilar regions were placed in 4% (w/v) PFA or snap-frozen in liquid nitrogen. The latter samples were stored at −80 °C until used.

Retrospectively, the diagnosis of IPF or fNSIP was reviewed and validated by A. Guenther and an expert pathologist (L. Fink) using current American Thoracic Society/European Respiratory Society (ATS/ERS) guidelines [1–4], and patients were included only when current ATS/ERS criteria were met. The study protocol was approved by the Ethics Committee of the Justus-Liebig-University School of Medicine (No. 31/93, 84/93, 29/01). Informed consent was obtained in written form from each subject for the study protocol. Demographic and clinical data (lung function test parameters) on donor subjects or patients receiving transplantation in Vienna are summarized in Table 1 (upper panel).

### 2.2. Human bronchoalveolar lavage fluid (BALF)

Next to lung tissues, bronchoalveolar lavage fluids (BALF) were collected from additional patients with sporadic IPF (n = 6; mean age ± SD: 65.83 ± 13.48 years; 1 female, 5 males), sporadic fibrotic NSIP (fNSIP, n = 7; mean age ± SD: 61.14 ± 21.25 years; 3 females, 4 males) at the time of first diagnosis as well as from six healthy volunteers (HV, n = 6; mean age ± SD: 31.67 ± 16.95 years; 4 females, 2 males) in the Dept. of Internal Medicine, Giessen (A. Guenther). All subjects with IIP underwent bronchoscopy for diagnostic purposes. Flexible fiberoptic bronchoscopy was performed in a standardized manner as previously described [32]. One segment of the lingual or the right middle lobe was lavaged with a total volume of 200 mL sterile saline in 10 aliquots. The fractions were pooled, filtered through sterile gauze, and centrifuged at 200 ×*g* (10 min, 4 °C) to remove cells and membranous debris. Aliquots of the cell-free BALF supernatant were stored at −80 °C. These patients undergoing BAL had not previously been treated with steroids or other immunosuppressants. Finally, a UIP—or fibrotic NSIP pattern was proven in all IPF—and NSIP subjects, because all of them later underwent video-assisted thoracic surgery (VATS) for diagnostic purpose. IIP-patients and HV gave their written informed consent to the study, and the local Ethics Committee approved the study. Demographic and clinical data (lung function test parameters) of these subjects are summarized in Table 1 (lower panel).

### 2.3. Sample preparation for two-dimensional gel analysis/DIGE technique

For the proteome analysis, peripheral lung tissue samples from the lower lobe, from the subpleural region of the lung was used. Frozen lung tissue samples (size 1 $cm^3$) from IPF-, fNSIP patients and controls were homogenized in extraction buffer, as described previously [33]. Crude lung extracts were centrifuged at 10,000 ×*g* for 10 min at 4 °C to remove cell debris. The protein concentration in each supernatant lung homogenate was determined according to the BCA protein assay from Perbio Science. Thereafter, equal masses of total protein (0.5 mg) of each individual IPF-, fNSIP- or control homogenate were pooled, respectively.

For isoelectric focusing (IEF), proteins were then precipitated with acetone (80% final concentration). After brief air drying in the hood, precipitated proteins of the IPF-, fNSIP- and control pool were resolubilized using a rehydration buffer containing 7 mol/L urea, 2 mol/L thiourea, 0.5% (v/v) pharmalyte buffer for commercial pH 4–7 and pH 6–11 linear IPG strips (GE Healthcare, Uppsala, Sweden), 4% (w/v) CHAPS and 20 mmol/L Tris. The concentration was adjusted for all pools to approx. 1.5 μg/μL. The resulting protein samples (in a volume of 2 mL) were frozen at −80 °C. The consecutive DIGE-proteome analysis was then undertaken with the help of TOPLAB GmbH, a proteomics company (Martinsried, Germany). In brief, the protein concentration in each pool was again determined by a commercially available kit. Thereafter, 50 μg proteins of each pool were labelled with 400 pmol of different CyDye fluorophors (IPF: Cy3, fNSIP: Cy5, control lungs: Cy2). The Cy2-, Cy3- and Cy5-labelled samples were subsequently combined and separated by using Two-dimensional gel electrophoresis (2D-PAGE). The separation was carried out on Multiphor™ II (GE Healthcare) in the first dimension (IEF electrophoresis, pH 4–7), followed by equilibration and reduction of IEF-strips according to standard protocols. Focused IPG gel strips were then loaded on top of SDS-polyacrylamid gels (13% total acrylamide, 3% bisacrylamide), and the second dimension electrophoresis was carried out using a Hoefer-ISO-DALT vertical gel electrophoresis system (GE Healthcare) according to standard procedures. The resulting 2D-DIGE-gel representing three different proteomes was performed in duplicate. It has to be noted that we did not perform the classical DIGE procedure by preparing an internal standard (pool of all samples) labelled with Cy2; instead, the control lung protein pool was labelled with Cy2 and served as the healthy, normal reference lung

**Table 1 – Selected demographic and clinical data on study subjects.**

| Explanted lung tissues | Organ donors (n = 10) | Sporadic IPF/UIP (n = 14) | Sporadic fNSIP (n = 8) |
|---|---|---|---|
| Mean age (yr ± SD) | 46.20 ± 18.25 | 54.29 ± 14.40 | 51.25 ± 8.52 |
| Gender (m/f) | 5/5 | 10/4 | 3/5 |
| FVC, % predicted (mean ± SD) | n.a. | 58.41 ± 12.54 | 50.7 ± 22.29‡ |
| $FEV_1$, % predicted (mean ± SD) | n.a. | 63.28 ± 9.47 | 47.1 ± 19.48‡ |
| Smoking status: current/former/never | n.a. | 0/7/7 | 0/1/6‡ |
| PY (mean ± SD) | n.a. | 37 ± 25 | n.a. |
| **Bronchoalveolar lavage fluids (BALF)** | **Healthy volunteers (HV, n = 6)** | **Sporadic IPF/UIP (n = 6)** | **Sporadic fNSIP (n = 7)** |
| Mean age (yr ± SD) | 31.67 ± 16.95 | 65.83 ± 13.48 | 61.14 ± 21.25 |
| Gender (m/f) | 2/4 | 5/1 | 4/3 |
| FVC, % predicted (mean ± SD) | 97.88 ± 8.59 | 68.92 ± 13.30†, § | 60.60 ± 13.64§ |
| $FEV_1$, % predicted (mean ± SD) | 103.15 ± 11.49 | 77.28 ± 11.93†, § | 65.25 ± 17.17§ |
| %DLC0/SB, % (mean ± SD) | 86.06 ± 11.77† | 39.14 ± 11.77†, § | 54.20 ± 10.64*, § |
| Smoking status: current/former/never | 0/0/6 | 0/3/2† | 0/2/5 |
| PY (mean ± SD) | – | 10 ± 14 | 2 ± 3 |

*Definition of abbreviations*: IPF = idiopathic pulmonary fibrosis; UIP = usual interstitial pneumonia; fNSIP = fibrotic non-specific interstitial pneumonia; BALF = Bronchoalveolar lavage fluid; FVC = forced vital capacity; $FEV_1$ = forced expiratory volume after 1 s; %DLCO/SB = ratio of diffusing capacity for carbon monoxide, single breath; PY = pack years; n.a. = not available.
‡ = In these cases, data were available from 7 individuals; † = In these cases, data were available from 5 individuals; * = $p < 0.05$ vs. IPF; § = $p < 0.01$ vs. HV.
With regard to explanted lung tissues, no data were available for DLCO/SB.

proteome. Because of the intention to analyze three different proteomes on one 2D-gel we chosed this strategy.

### 2.4. *Image analysis of two-dimensional-DIGE-gels*

After 2D-PAGE, gels were scanned with 100 μm resolution using the Ettan™ DIGE Imager. Excitation wavelengths and emission filters were chosen specifically for each of the CyDyes, and images with DIGE readouts Cy2, Cy3 and Cy5 were recorded (Supplementary Fig. E1).

Computer-assisted analysis of imaged 2D-gels/DIGE readouts was performed with Proteom Weaver Software (v 3.0.0.3, BioRad, Munich, Germany). In brief, spot detection, matching of protein/peptide spots between gels and different readouts ("in-gel spot-codetection"), as well as background subtraction and normalization etc. were carried out by the software using standard settings. Individual spot intensities were calculated by the software. For the comparative analysis of the different CyDye labelled lung proteomes, three distinct overlays of the respective readouts were performed (Control-Cy2/IPF-Cy3, Control-Cy2/fNSIP-Cy5 and fNSIP-Cy5/IPF-Cy3). The spots qualifying for differential protein expression had the following criteria: correct positioned matching in all gels and readouts, expressed with 95% statistical confidence ($p$-value < 0.05, unpaired Student´s $t$ test). Additionally, for the comparison of the IPF- and the fNSIP-proteome with regard to the control proteome, protein spots were considered as differentially regulated if the -fold change value (quotient of corresponding group means of spot intensities, also designated as regulation factor RF) between the IPF- and the control group, as well as between the fNSIP- and control group, was ≥1.5 (for 1.5-fold or more upregulation) or ≤0.75, (for 1.5-fold or more downregulation). The same criterion was used for the comparison of the fNSIP-proteome with regard to the IPF-proteome. The criterion meaning a ≥1.5-fold change in expression between the comparison groups was chosen, due to the relative low number of differentially regulated proteins fulfilling a 2.0-fold change (especially the downregulated proteins), and because there was nearly no spot revealing two-fold or more differential regulation in the comparison fNSIP versus IPF. For an overview, scatterblots were performed in which the intensities of the "matched" protein spots in the respective overlays were compared (IPF-Cy3 versus Control-Cy2, fNSIP-Cy5 versus Control-Cy2 and fNSIP-Cy5 versus IPF-Cy3) [see Supplementary Figs. E2 and E3] using the "default setting". The scatterblots for the comparisons IPF-Cy3 versus Control-Cy2 [Suppl. Fig. E2A] and fNSIP-Cy5 versus Control-Cy2 [Suppl. Fig. E2B] indicated evidently similar amounts of differentially regulated proteins in both entities with regard to the control proteome. Interestingly, in the comparison fNSIP versus IPF, only a sparse amount of protein spots revealed differential regulation (Suppl. Fig. E3). The spot quantities and regulation factors for the comparison IPF and fNSIP versus control group are summarized in Supplementary Table E1, and these for the comparison fNSIP versus IPF in Supplementary Table E2.

Due to low abundance of differential regulated protein spots in 2D-DIGE-PAGEs, micropreparative 2D-PAGE´s using 600–1000 μg lung proteins (from the fNSIP pool or from a 1:1 mixture of the fNSIP pool with the control lung pool, both "mixtures" contained wholly all differential regulated protein spots identified by DIGE-image analysis) were performed and stained with coomassie, in order to guarantee enough protein content for the identification by MALDI-TOF-MS.

### 2.5. *Protein digestion and MALDI-TOF-MS analysis*

In brief, the selected spots were excised and trypsin digested according to standard protocols. Prior to digestion, the proteins were destained using 50 mM $(NH_4)HCO_3$ in 30% acetonitrile. In-gel digestion was performed overnight with 0.05–0.15 μg trypsin sequencing grade (Roche Diagnostics, Mannheim, Germany 2006, Serva 2011) in 10 mM $(NH_4)HCO_3$. The resulting peptide mixture was desalted using μ $C_{18}$ ZipTips (Millipore,

Bedford, MA) according to the manufacturer´s instructions. Then the desalted peptide mixture was spotted onto a stainless steel target (AB Sciex) using the dried droplet method with the matrix alpha-cyano-4-hydroxy cinnamic acid. The peptides on the target were measured with a MALDI mass spectrometer (4800 Proteomics Analyzer, AB SCIEX, Foster City, CA, USA). The spectrum was acquired in the mass range of 700–4.500 m/z (2006: 600–4.200 m/z) with the instrument operating in reflection mode.

The raw spectra were processed with the Data explorer (version 4.3.; AB Sciex) software. All spectra were externally calibrated using a peptide calibration standard (AB Sciex 2006, Bruker 2011). Database queries of the monoisotopic masses were performed with the search engine ProFound (prowl.rockefeller.edu), which uses the Bayesian probability to identify unknown sequences against a protein sequence database. ProFound takes into account individual properties of each protein in the database as well as other information relevant to the experiment such as the mass range in which the protein is expected to lie (this information can be taken from 2D-gel).

The sequence database to be searched was the NCBI non-redundant database (the version released in Sep. and Nov. 2007, and Feb. 2012). The taxonomic category was "Homo sapiens (human)" (119130 sequences). The other search parameters were $M_r$ ranges within ±25% of measured values, pI range from 0.0 to 14.0, monoisotopic peptide masses, one missed cleavage by trypsin, complete modifications: iodoacetamide-C, partial modifications: oxidation (M), charge state: MH+, and mass accuracy: 100.00 ppm. The criterium used for a positive identification was a significant Z-score (Est´dZ) with the probability score 1.0e+000. To date, proteins reaching a ProFound score ≥1.65 are considered as significant at the 5% level ($P < 0.05$). Of the databases for peptide mass fingerprints (PMFs), Mascot and ProFound have been shown to clearly separate the correct identifications from the random matches.

The PMF mass spectra and protein identification results of the proteins identified in this study are shown in Supplemental Figs. S1 to S36; including MS-peak list, Z-score, the number of peptides matched to the identified protein from the total of peptides submitted, the sequence coverage, theoretical MW and pI of the identified protein, and the mass tolerance of matched peptides.

### 2.6. Immunohistochemistry (IHC)

Human lungs were placed in 4% (w/v) paraformaldehyde after explantation (fixation was done for 12–24 h), and processed for paraffin embedding. Sections (3 μm) were cut, mounted on positively charged glass slides (Super Frost Plus, Langenbrinck), and subjected to antigen retrieval by cooking the sections in 10 mmol/L sodium citrate (pH 6.0) as previously described [33]. Proteins of interest were visualized using the ZytoChem-Plus AP Kit (Fast Red) or ZytoChem-Plus HRP Kit (DAB-staining, brown dye), Broad Spectrum (Zytomed Systems, Berlin, Germany) according to protocols of the manufacturer. In the following, the primary antibodies used for IHC are listed, including the sources and dilutions: rabbit polyclonal for human proSP-C (1:750, Millipore), rabbit monoclonal for cytokeratin-5 [KRT5] (1:200, abcam), rabbit polyclonal for human PPIA (1:100, Santa Cruz Biotechnology Inc.), mouse monoclonal for human LAP3 (1:100, Santa Cruz B. I.), rabbit polyclonal for human PSME1/PA28α (1:500, Calbiochem), rat monoclonal for human clara cell-protein 10 [CC10] (1:75, R&D Systems), mouse monoclonal for human FoxJ1/HFH4 (1:75, Abcam), rabbit polyclonal for CD68 (1:200, Abcam), rabbit polyclonal for human Prdx1 (1:800, Abcam), rabbit polyclonal for human ATF6/p50ATF6 (1:100, Abcam), rabbit polyclonal for human XBP1 (1:50, Santa Cruz B. I.), mouse monoclonal for human Prdx6 (1:1000, Abcam) and rabbit polyclonal for cytokeratin-19 [KRT19] (1:100, Abcam). Control sections were treated with PBS or with rabbit or mouse primary antibody isotype control (Acris Antibodies GmbH, Hiddenhausen, Germany) to determine the specificity of the staining.

Lung tissue sections were scanned with a Mirax Desk slide scanning device (Mirax Desk, Zeiss, Göttingen, Germany), and examined histopathologically at 100×, 200× and 400× original magnification. IHC for mentioned antibodies was undertaken in 10 IPF-, 5 fNSIP- and 8 control lung samples.

### 2.7. Quantitative Western Blot analysis of human BALF and statistics

The protein concentration in BALF was determined according to the BCA protein assay from Perbio Science, followed by concentration of BALF samples to 5 or 10 μg lavage protein per case using a SpeedVac concentrator. Samples were then each dissolved in 20 μL of SDS-sample buffer (final concentration 2% (w/v) SDS, 2.5% (v/v) β-mercaptoethanol, 10% (v/v) glycerol, 12.5 mmol/L Tris–HCl [pH 6.8], 0.1% (w/v) bromophenol blue) and immersed in boiling water for 10 min, followed by separation on 10%-, 12%- or 15% SDS-PAGEs. Thereafter, separated proteins were transferred in a semi-dry blotting chamber to PVDF membranes (GE Healthcare), followed by immunostaining for LAP3 (diluted 1:250), Prd×1 (diluted 1:1000), Prd×6 (diluted 1:500), serum amyloid P component [SAP] (rabbit polyclonal, abcam, diluted 1:40,000) and KRT19 (diluted 1:200) with use of respective horseradish peroxidase-conjugated secondary antibodies (DakoCytomation, Hamburg, Germany; rabbit anti-mouse-IgG and swine anti-rabbit IgG, both diluted 1:2000). Blot membranes were developed with the ECL Plus chemiluminescent detection system (GE Healthcare), and emitted signals were detected with a chemiluminescence imager (Intas ChemoStar, Intas, Göttingen, Germany). Thereafter, band intensities in acquired TIFF/JPEG-images were analyzed by densitometric scanning and quantified using ImageJ software (Version 1.45 s, NIH).

For the statistical comparison of differences between two groups (IPF vs. HV, fNSIP vs. HV and fNSIP vs. IPF) the non-parametric Mann–Whitney *U*-test was applied using the software GraphPad Prism version 4.0 (GraphPad Software Inc., La Jolla, CA). Data are presented as mean ± SEM of the individual values of different subjects. A p-value < 0.05 was considered statistically significant.

## 3. Results

### 3.1. Comparative proteomic analysis of IPF and fibrotic NSIP versus Control lung tissues

For comparative proteomic profiling of IPF- (n = 14), fNSIP- (n = 8) and control lungs (n = 10), equal protein concentrations of lung

homogenates of each patient group and the control group were pooled in order to identify reproducible and robust differences. Differential labelling with three distinct fluorescent dyes was carried out resulting in a Cy3-labelled IPF-, a Cy5-labelled fNSIP- and a Cy2-labelled control lung proteome. The subsequent comparison of the fNSIP proteome with regard to the control lung pattern revealed 26 differentially regulated proteins which differed more than or equal to 1.5-fold, of which 14 were upregulated (RF ≥ 1.5, Table 2) and 12 downregulated in fNSIP (RF ≤ 0.75, Table 3). A similar regulation was observed for 24 out of these 26 protein spots in the comparison IPF versus controls (Tables 2 and 3). Both tables provide information about the identification of these differently expressed protein spots, as well as the magnitude of difference versus the control group (indicated as RF). Additionally, all differentially regulated proteins for the comparison IPF- and fNSIP- versus control proteome are depicted in the proteome map in Fig. 1A. It has to be noted that some of the identified proteins (TPIS, KRT19, CTSD) occurred on several positions in the 2D-gel suggesting the occurrence of protein isoforms/variants. The isoforms/variants of one protein were not observed in each case to be regulated in the same manner as reflected (in part) by varying spot intensities/RF-values.

The major part of the proteins we identified as being upregulated in IPF and fNSIP fall into the related categories chaperone/protein folding (PPIA), protein processing (LAP3), energy generation/glycolysis (TPIS) and antioxidant function (PRDX1) (Table 2), and could be all assigned also as stress-induced genes. Genes involved in epithelial cytoskeletal organization such as cytokeratin-19 (KRT19) were also found to be increased in IPF and fNSIP (Table 2).

### 3.2. *Upregulated stress-induced genes in IPF and fibrotic NSIP and their localization in lung epithelium*

The accumulation of the Unfolded Protein Response (UPR) chaperone peptidyl-prolyl cis-trans isomerase A (PPIA) was validated by immunohistochemistry (IHC) in order to identify the cellular distribution in fNSIP-, IPF- and control lung tissues. In addition, we performed staining for prosurfactant protein C (proSP-C), a protein specific to AECII, of parallel sections, in order to designate alveolar structures in these lung tissues (Fig. 2A–D, and O). A very strong overexpression of PPIA was observed in AECII in areas of thickened alveolar septae in fNSIP (Fig. 2E, F) as well as in AECII overlying dense zones of fibrotic remodelling in IPF/UIP lungs (Fig. 2G, H), which was in contrast to AECII in control lungs with normal histological appearance (Fig. 2P) indicating no or only a faint PPIA expression. Interestingly, bronchiolar basal cells (which were characterized by cytoplasmic cytokeratin-5/KRT5 staining) in abnormal bronchiolar structures such as basal cell hyperplasia (Fig. 2I) or hyperplastic bronchioles (Fig. 2J) also revealed a pronounced expression of PPIA (Fig. 2L, M) which was only weak or barely detectable in the basal proportion of normal lung tissues (Fig. 2K, N). Basal cells in bronchioles of fNSIP lungs, which have a less abnormal bronchiolar tree as compared to IPF/UIP also showed a prominent expression of PPIA (not shown). Fibroblastic cells revealed no or minimal immunostaining for PPIA, whereas interstitial inflammatory cells (mast cells, lymphocytes) in both—fibrotic and normal lung—also showed considerable expression of PPIA (Fig. 2E–H, L–N).

Next, we went on to characterize the localization of expression of LAP3, a cytosolic leucine aminopeptidase involved in processing of antigenic proteins [34], in the fibrotic—and normal lung. Similar to PPIA and in line with its observed upregulation in fNSIP and IPF (Table 2), a robust LAP3 expression was predominantly found to co-localize with the proSP-C expression in the AECII in areas of thickened alveolar septae in fNSIP (Fig. 3A, B, E, F) as well as in AECII near dense zones of fibrosis in IPF lungs (Fig. 3C, D, G, H), whereas AECII of control lungs with normal alveolar architecture indicated a basal, lower level of expression of LAP3 (Fig. 3M-P). No notable staining was observed in fibrotic tissue itself, but inflammatory cells in the interstitium as well as macrophages in fibrotic and normal lungs revealed

**Table 2 – Proteins significantly upregulated in IPF and fNSIP lungs relative to control lung tissue (RF ≥ 1.5).**

| Spot no: | Accession number (NCBI)/Protein name | Score/ Est´d Z (Z-score) | Seq. cov. (%) | Matched peptides | Theor. MW [kDa] | RF_IPF/ donor | RF_ NSIP/ donor |
|---|---|---|---|---|---|---|---|
| 3158 | gi\|11493459: PRO2619, serum albumin (ALB) | 2.06 | 32 | 18 | 58.53 | 5.7869 | 5.4891 |
| 3012 | gi\|37588925: LAP3 protein, Leucine aminopeptidase | 2.42 | 54 | 22 | 54.77 | 3.3611 | 2.4152 |
| 3104 | gi\|15277503: ACTB protein | 2.24 | 32 | 10 | 40.54 | 2.1605 | 2.8496 |
| 3064 | gi\|999892: Triosephosphate isomerase (TPIS) | 2.37 | 90 | 21 | 26.81 | 3.2599 | 3.8891 |
| 2981 | gi\|178777: Proapolipoprotein A-1 preproprotein (APOA1BP) | 2.32 | 43 | 12 | 30.75 | 2.3927 | 2.2229 |
| 3032 | gi\|55959887: peroxiredoxin 1 (PRDX1) | 2.26 | 51 | 8 | 19.13 | 2.8129 | 2.7443 |
| 2780 | gi\|20149498: ferritin, light polypeptide | 2.37 | 63 | 14 | 20.03 | 2.3630 | 3.0931 |
| 3550 | gi\|4503571: enolase 1 (ENO1) | 2.27 | 61 | 22 | 47.49 | n.a. | 4.6511 |
| 2881 | gi\|24234699: keratin 19 (KRT19) | 2.36 | 41 | 17 | 44.09 | 6.2736 | 6.0776 |
| 3089 | gi\|4501883: alpha 2 actin (ACTA2) | 2.25 | 50 | 12 | 42.39 | 1.6950 | 2.1342 |
| 2922 | gi\|999892: Triosephosphate isomerase (TPIS) | 2.31 | 79 | 18 | 26.81 | 2.8328 | 3.6807 |
| 3219 | gi\|1431788: Cyclophilin A, peptidylprolyl isomerase A (PPIA) | 2.37 | 55 | 17 | 18.09 | 2.3102 | 2.1868 |
| 2719 | No significant identification | – | – | – | – | 6.0894 | 8.6522 |
| 3178 | No significant identification | – | – | – | – | 5.1576 | 4.9577 |

*Definition of abbreviations*: RF = regulation factor; Est´d Z: Z-score/Profound score: a Z-score of ≥1.65 is considered significant at the 5% level ($p < 0.05$); Seq. cov. (%) = sequence coverage in %; Theor. MW [kDa] = theoretical molecular weight in kDa; n. a. = not applicable.

**Table 3 – Proteins significantly downregulated in IPF and fNSIP lungs relative to control lung tissue (RF ≤ 0.75).**

| Spot no. | Accession number (NCBII)/Protein name | Score/ Est´d Z (Z-score) | Seq. cov. (%) | Matched peptides | Theor. MW [kDa] | RF_ IPF/ donor | RF_ NSIP/ donor |
|---|---|---|---|---|---|---|---|
| 2799 | gi\|809185: Annexin 5, ANXA5, Lipocortin V, Placental anticoagulant protein 1 (PAP-I) | 2.30 | 64 | 23 | 35.84 | 0.5296 | 0.5556 |
| 3170† | gi\|4503143: Cathepsin D preproprotein (CTSD) | 2.32 | 34 | 12 | 45.05 | 0.5674 | 0.5717 |
| 2949 | gi\|576259: Serum amyloid P component (SAP) | 2.30 | 40 | 8 | 23.35 | 0.5318 | 0.5829 |
| 3077 | gi\|87564: glutathione transferase (EC 2.5.1.18) (GST) | 1.43 | 56 | 7 | 23.44 | 0.4891 | 0.5420 |
| 2854 | gi\|306880: preprohaptoglobin, haptoglobin (HPT) | 2.11 | 33 | 8 | 38.95 | 0.6025 | 0.4849 |
| 2959 | gi\|13787109: Alpha-1-antitrypsin (A1AT) | 2.18 | 29 | 11 | 44.32 | 0.8358 | 0.5253 |
| 3232 | Mixture: | | | | | 0.8242 | 0.6957 |
| | 1. gi\|28949044: mitochondrial Aldehyde dehydrogenase (ALDH2) | 2.29 | 52 | 14 | 54.94 | | |
| | 2. gi\|16306550: selenium binding protein 1 (SBP1) | 1.70 | 32 | 8 | 52.94 | | |
| 2907# | P60709/ACTB_HUMAN: Actin, cytoplasmic 1, beta-actin or P63261/ACTG_HUMAN: Actin, cytoplasmic 2, gamma-actin | 124 (MOWSE score) | 51 | 13 | 42.05 42.11 | 0.4180 | 0.3387 |
| 2900 | gi\|4557581: Fatty acid-binding protein 5 (FABP5) | 1.73 | 58 | 7 | 15.49 | 0.3534 | 0.3883 |
| 2903* | gi\|5032057: S100 calcium binding protein A11 (S100A11) | 2.15 | 87 | 8 | 11.84 | 0.5659 | 0.4155 |
| 3107 | No significant identification | – | – | – | – | 0.5459 | 0.5686 |
| 2807 | No significant identification | – | – | – | – | 0.4743 | 0.4467 |

Definition of abbreviations: RF = regulation factor; Est´d Z: Z-score/Profound score: a Z-score of ≥1.65 is considered significant at the 5% level ($p < 0.05$); Seq. cov. (%) = sequence coverage in %; Theor. MW [kDa] = theoretical molecular weight in kDa.
† = spot migrates with MW ~ 31 kDa in 2-DE, Cathepsin D heavy chain identified; * = only identified using up to 30 kDa range;
# = identified with Mascot/Swiss-Prot database version 20110609.

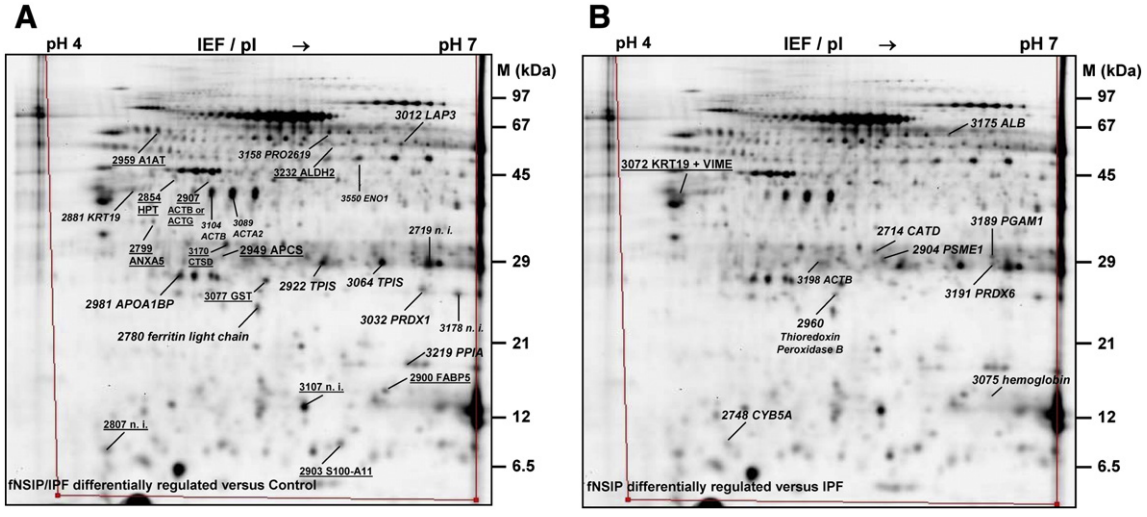


**Fig. 1 – Representative reference 2D-gels of 1000 μg lung proteins mapping differentially regulated proteins in (A) the comparison fNSIP/IPF- versus Control lung proteome and (B) the comparison fNSIP- versus IPF proteome. (A) Separation of proteins from a 1:1 mixture of the fNSIP—and Control lung proteome pool (which contained wholly all differentially protein spots identified by precedent DIGE-image analysis) was performed on linear strips with a pH range of 4–7 followed by 16% SDS-PAGE. The 2D-gel was stained with Coomassie. Proteins upregulated in fNSIP and IPF versus Control are indicated in italic font, downregulated proteins are underlined. Differentially expressed protein spots which could not be successfully identified, are indicated with n. i. (= not identified). (B) The same 2D-separation setting as shown in (A) was performed, followed by staining of the 2D-gel with Coomassie. Proteins upregulated in fNSIP versus IPF are indicated in italic font, downregulated proteins are underlined. Both 2D-gels were used as reference proteomes, for excising and MS identification of the differentially regulated protein spots.**

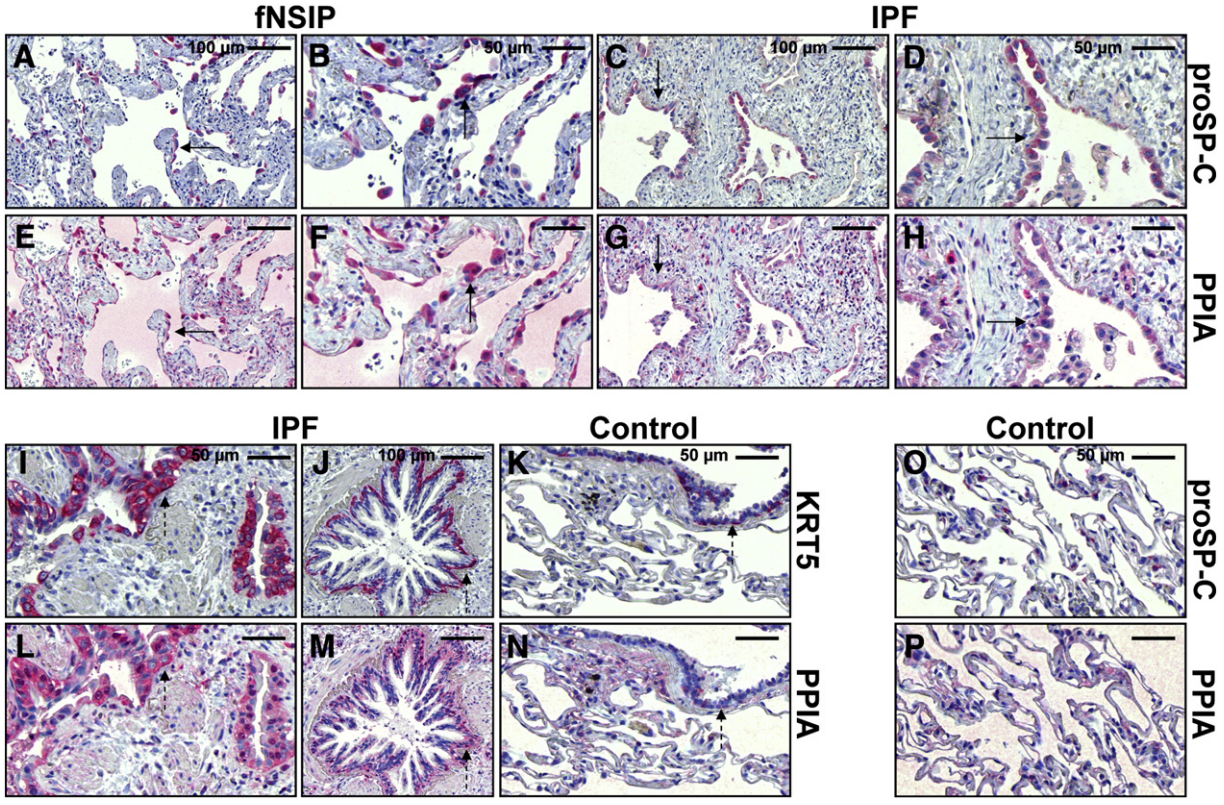


**Fig. 2 – Upregulation of peptidylprolyl isomerase A (PPIA) expression in type-II alveolar epithelial cells (AECII) in fibrotic NSIP- and IPF lungs. Representative immunohistochemistry for proSP-C (A–D), cytokeratin-5 [KRT5] (I, J) and PPIA (E–H, L, M) in serial sections of fNSIP- and IPF lung tissues, and for proSP-C (O), KRT5 (K) and PPIB (N, P) in control lungs. (E, F, P) In fibrotic NSIP lungs (fNSIP), type-II alveolar epithelial cells (AECII) in areas of thickened alveolar septae reveal strong induced expression of PPIA (E, F), in comparison to control lungs which indicate only faint expression of PPIA (P). (G, H, P) AECII near dense zones of fibrosis in IPF lungs indicate upregulated expression of PPIA, when compared to control lungs. AECII are indicated by proSP-C staining (A–D) and arrows in A–H. (L, M, N) Robust overexpression of PPIA is also observed in bronchiolar basal cells of epithelial abnormalities such as basal cell hyperplasia (L) or hyperplastic bronchioles (M) in IPF lungs (indicated by cytoplasmic KRT5-staining in serial sections I and J, and by dashed arrows in L and M), whereas basal cells of control lungs indicate only less immunoreactivity for the PPIA antibody (N). Original magnification of photomicrographs A, C, E, G, J and M: ×200 (bar = 100 µm); original magnification of photomicrographs B, D, F, H, I, K, L, N, O and P: ×400 (bar = 50 µm).**

also considerable expression of LAP3 (Fig. 3G, H, and N). Furthermore, ciliated bronchial cells (as indicated by dashed arrows in Fig. 3I–L and parallel immunostaining with the marker FoxJ1 in Fig. 3K), but not non-ciliated clara cells (indicated by CC10 staining in Fig. 3J), revealed a strong apical staining pattern of LAP3 in IPF (Fig. 3I), fNSIP- (not shown) and control lungs (Supplementary Fig. E4), supporting secretion of this aminopeptidase. Quantitative immunoblot analysis of bronchoalveolar lavage fluids for LAP3 indicated evident extracellular appearance of this enzyme in fNSIP-, IPF- and normal lungs, but no statistical significant differences between the three categories in secretion of LAP3 (Supplementary Fig. E5).

Another stress-induced gene found to be upregulated in fNSIP and IPF was the antioxidant protein peroxiredoxin 1 (PRDX1). By IHC, PRDX1 expression was predominantly found in ciliated bronchial cells in IPF lungs (Fig. 4B, brown staining), which were clearly marked by nuclear FoxJ1 staining in a parallel section (Fig. 4D), whereas non-ciliated clara cells (indicated by CC10 staining in Fig. 4C) did not express this enzyme (Fig. 4B). Furthermore, AECII near regions of dense fibrosis of IPF lungs (indicated by proSP-C staining in Fig. 4A, F) revealed also no significant expression of PRDX1 (Fig. 4B, G), even not after overstaining of lung tissues sections (Supplementary Fig. E6A + B). Instead, a strong PRDX1 overexpression was observed in alveolar macrophages (AM) of IPF—(Fig. 4G, AM are indicated by CD68 staining in Fig. 4H) and fNSIP lungs (Supplementary Figs. E6G + H), whereas AM in control lung tissues revealed no or faint expression of PRDX1 (Fig. 4J, K). Similarly, AECII in control lungs indicated no notable or only weak expression of PRDX1 (Fig. 4I, J), and only the ciliated bronchial epithelium expressed PRDX1 in basal amounts in normal lungs (Supplementary Fig. E6T). Interestingly and much to our surprise, AECII in areas of fibrotic, thickened alveolar septae of fNSIP lungs (Fig. 4L–N) indicated a pronounced induction and thus upregulation of PRDX1 expression (Fig. 4O–Q, indicated by arrows), and which was—similar to our IHC results in IPF—not observed in AECII near areas of dense uniform fibrosis in fNSIP lungs (not shown). Importantly, fibroblastic cells or fibroblast foci did not reveal a notable PRDX1 expression (not shown).

Due to reported appearance of PRDX1 and other peroxiredoxins in BALF of IIP patients [35–37], we next performed a quantitative immunoblot analysis of BALF samples

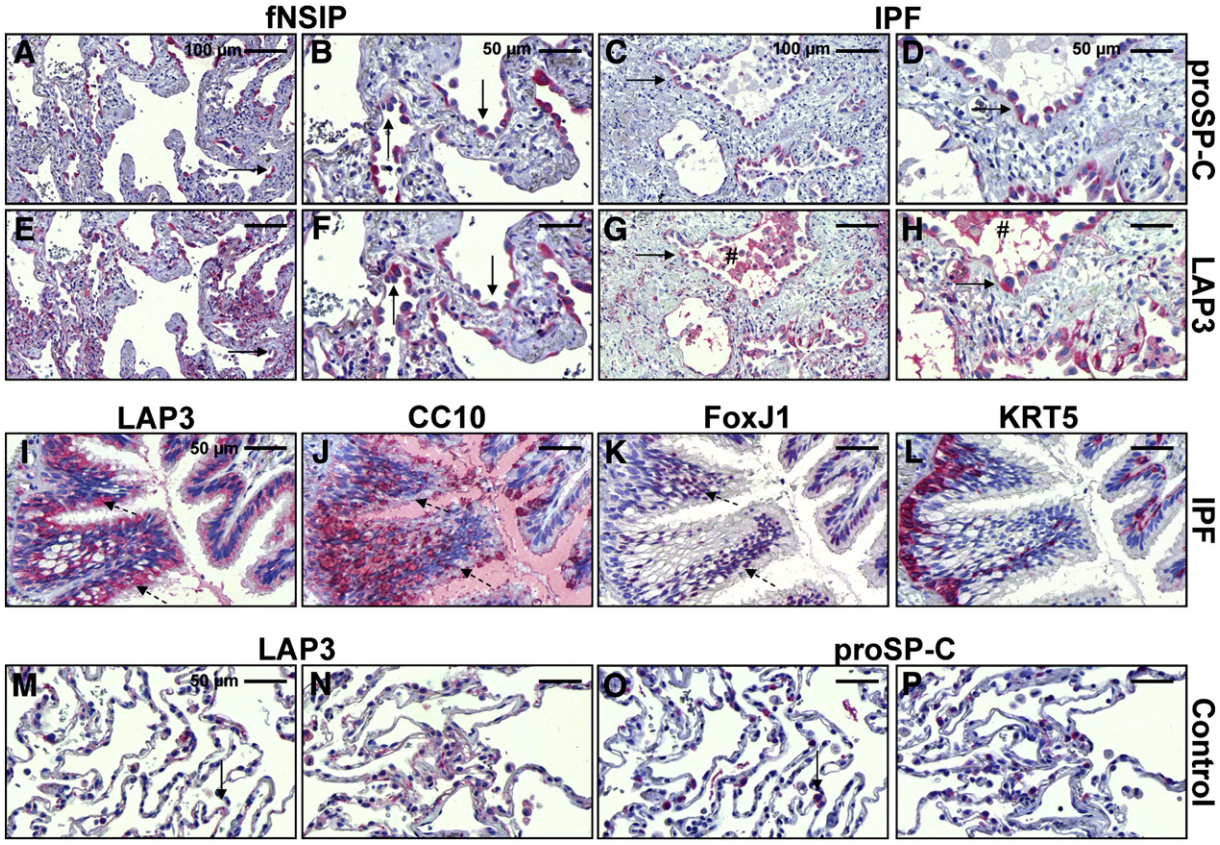


**Fig. 3 – Expression analysis of leucine aminopeptidase LAP3 in lung tissue from patients with fibrotic NSIP and IPF in comparison to Control lungs. Representative immunohistochemistry for proSP-C (A–D), LAP3 (E-I), clara cell-protein 10 [CC10] (J), FoxJ1 (K) and cytokeratin-5 [KRT5] (L) in serial sections of fNSIP- and IPF lung tissues, and for LAP3 (M, N) and proSP-C (O, P) in control lungs. (E, F, G, H) Type-II alveolar epithelial cells (AECII) in areas of thickened alveolar septae in fibrotic NSIP lungs (fNSIP; E, F) as well as AECII in regions of dense fibrotic remodelling in IPF lungs (G, H) reveal robust overexpression of LAP3. AECII are indicated by proSP-C staining (A–D) and arrows in A–H. LAP3 immunostaining is also observed in alveolar macrophages (indicated by hashmark in G and H). (I, J, K, L) Ciliated bronchial cells in IPF lungs express also LAP3 (I), as indicated by dashed arrows and immunostaining of serial sections with the marker protein FoxJ1 (K). Clara cells (marked by CC10 staining in Fig. J) do not express LAP3. The same observations can be made in control lungs (not shown) (M, N) AECII of control lungs (as indicated by proSP-C staining in parallel sections O and P) reveal a basal level of LAP3 expression. Original magnification of photomicrographs A, C, E, G: ×200 (bar = 100 µm); original magnification of photomicrographs B, D, F, H, I–L and M–P: ×400 (bar = 50 µm).**

from fNSIP- and IPF patients, as well as healthy volunteers (HV) for PRDX1. Representative immunoblot (Fig. 4R) and densitometric quantification (Fig. 4S) indicated an inconsistent and insignificant upregulation of extracellular PRDX1 levels in BALF of fNSIP- and IPF patients when compared to HV.

### 3.3. *Down-regulated proteins in IPF and fibrotic NSIP versus Control lung tissues*

Among the downregulated proteins in IPF and fNSIP were genes crucial for cell healthiness and survival, namely antioxidants (glutathione transferase, haptoglobin [HPT]) and anticoagulant proteins, such as annexin A5 (ANXA5), the latter being also involved in autophagy [38] (Table 3). Another interesting protein found to be downregulated in IPF and fNSIP was serum amyloid P component (SAP) which has been previously described as an inhibitor of fibrocyte differentiation [39,40] (Table 3). We therefore wanted to investigate the localization of biosynthesis of this very interesting enzyme in IPF-, fNSIP- and control lung tissues by IHC, but failed due to the nature of commercially available antibodies against SAP, which turned out to be not suitable for IHC. Due to its reported secretion, we performed comparative immunoblot analysis of BALF samples from IPF-, fNSIP patients and HV for SAP. SAP protein levels were significantly reduced in BALF from IPF patients in comparison to HV ($p < 0.05$, Fig. 5A and B), and were also evidently lower in comparison to fNSIP (without statistical significance, $p = 0.1014$). Interestingly, BALF contents of SAP did not differ significantly between the fNSIP—and HV group (Fig. 5A and B).

### 3.4. *Differentially regulated proteins in fibrotic NSIP versus IPF lungs and their localization in epithelium*

The subsequent comparison of the fNSIP - to the IPF lung proteome revealed 10 differentially regulated proteins which differed more than or equal to 1.5-fold, and of which nine

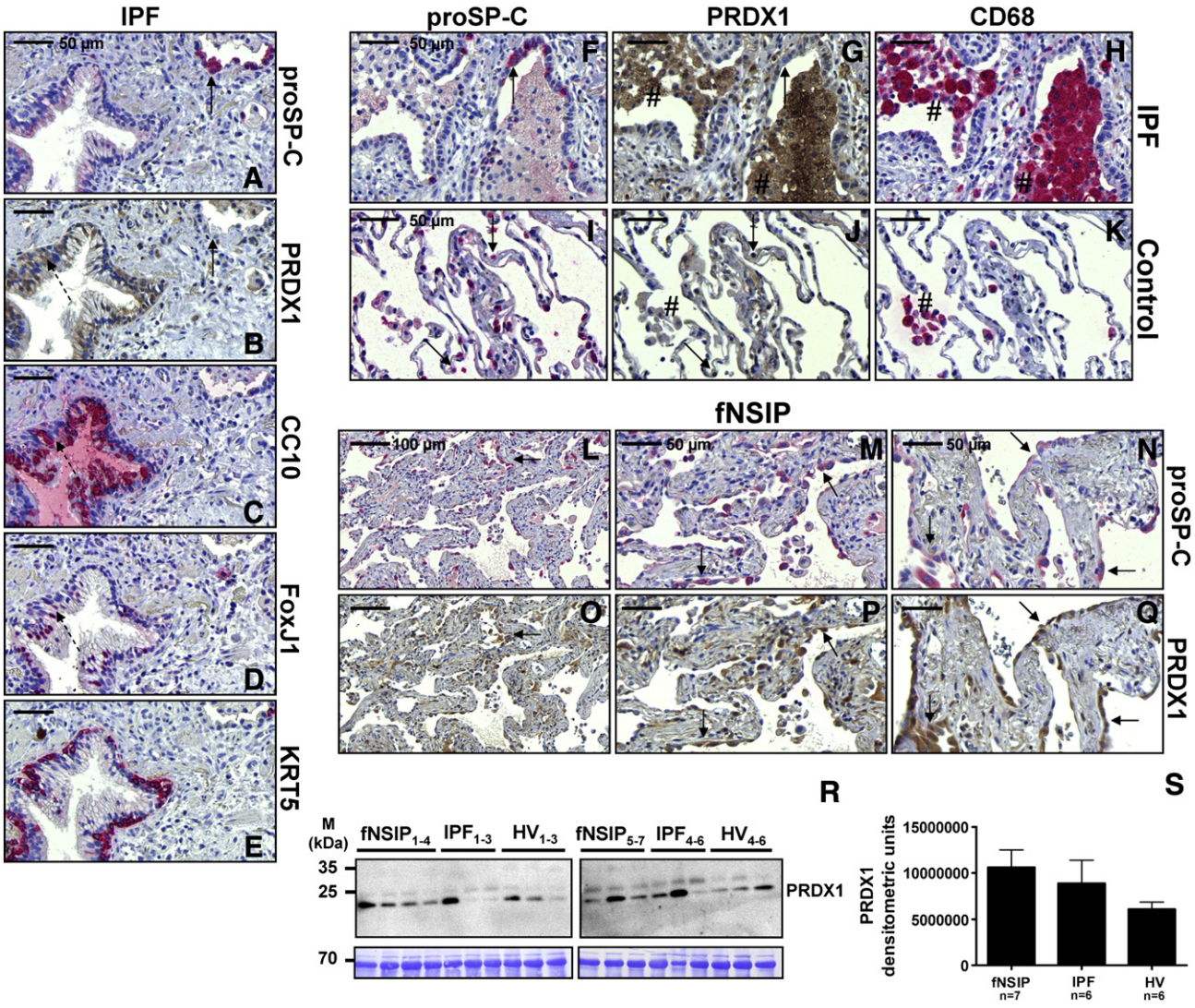


**Fig. 4 – Expression analysis of peroxiredoxin 1 (PRDX1) in lungs from patients with fibrotic NSIP and IPF in comparison to Control lungs. Representative immunohistochemistry for proSP-C (A, F, L–N), PRDX1 (B, G, O-Q), clara cell-protein 10 [CC10] (C), FoxJ1 (D), cytokeratin-5 [KRT5] (E) and CD68 (H) in serial sections of IPF- and fibrotic NSIP (fNSIP) lung tissues, and for proSP-C (I), PRDX1 (J) and CD68 (K) in control lungs. (A–E, F–K) In IPF, PRDX1 expression is localized to ciliated bronchial cells (B) which are indicated by FoxJ1-staining in a parallel section (D) and dashed arrows in figs. B and D. Non-ciliated clara cells (as indicated by CC10 staining in C) don´t express PRDX1 (dashed arrows in B and C). Prominent PRDX1 overexpression is observed in alveolar macrophages (marked by CD68 staining in H) in IPF lung tissues (indicated by hashmarks in figs. G and H), whereas AECII of IPF lungs (which are marked by proSP-C staining in serial sections A and F) do not show any notable expression of PRDX1 (indicated by arrows in A, B, F and G). AECII and alveolar macrophages in control lungs reveal no notable PRDX1 expression (AECII are indicated by arrows in I and J, macrophages with hashmarks in J and K). (L–Q) In contrast to AECII of IPF- and control lungs, robust induction of PRDX1 expression is observed in AECII in areas of thickened alveolar septae in some fNSIP lungs (indicated by arrows in L–Q). Original magnification of photomicrographs A–K, M, N, P, Q: ×400 (bar = 50 µm); original magnification of photomicrographs L and O: ×200 (bar = 100 µm). (R) Representative immunoblot and (S) quantitative immunoblot analysis for PRDX1 of BAL fluid from patients with sporadic fNSIP (n = 7), IPF (n = 6) and healthy volunteers (HV, n = 6). Five µg protein of cell-free BALF samples were concentrated and separated on a 12% SDS-PAGE. Coomassie staining of the blot membrane was used as a loading control. Intensity of bands was densitometrically quantified and presented as column diagram for each category (mean ± SEM).**

were upregulated (RF ≥ 1.5, Table 4) and one downregulated in fNSIP (RF ≤ 0.75, Table 4). Table 4 provides information about the identification of these differently expressed protein spots, as well as the magnitude of difference with the IPF group (indicated as RF). As additional information, the RF values for the relations fNSIP vs. controls as well as IPF vs. controls are given for these spots in Table 4, because these "differentially regulated in fNSIP vs. IPF spots" were often upregulated in both entities relative to control lungs. For an overview, all differentially regulated proteins for the comparison fNSIP-

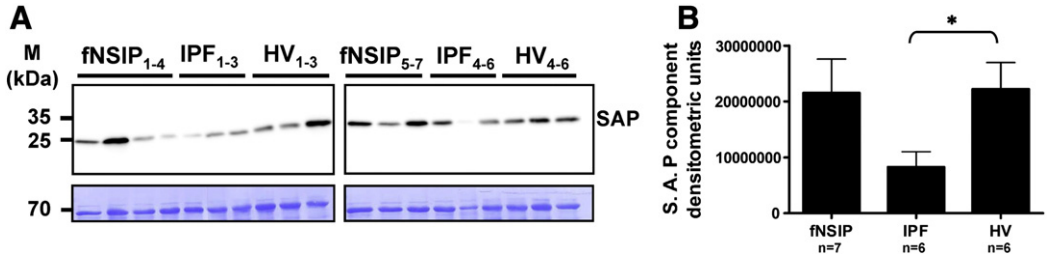


**Fig. 5 – Serum amyloid P component in human bronchoalveolar lavage fluid (BALF) from patients with fibrotic lung disease and healthy volunteers. (A) Representative immunoblot and (B) quantitative immunoblot analysis for SAP of BAL fluid from patients with sporadic fNSIP (NSIP, n = 7), IPF (n = 6) and healthy volunteers (HV, n = 6). Five μg protein of cell-free BALF samples were concentrated and separated on a 12% SDS-PAGE. Coomassie staining of the blot membrane was used as a loading control. Intensity of bands was densitometrically quantified and presented as column diagram for each category (mean ± SEM). * ($p < 0.05$) for fNSIP versus HV.**

versus IPF proteome are depicted in the proteome map in Fig. 1B.

Most of the proteins we identified as being upregulated in fNSIP versus IPF appeared to be involved in defense mechanisms against oxidative stress, namely antioxidants (PRDX6, thioredoxin peroxidase B) or were activators of the proteasome (PSME1). Genes involved in energy generation such as glycolytic enzymes (PGAM1) were also found to be upregulated in fNSIP relative to IPF (Table 4).

First, we investigated the expression of proteasome activator complex subunit 1 (PSME1), which appeared to be upregulated in fNSIP relative to IPF- and control lungs, and the expression of which did not seem to differ between IPF and controls according to the DIGE analysis (Table 4), by IHC in respective lung tissues. AECII of thickened alveolar septae in fNSIP lungs (Fig. 6A-D) revealed a strong induction of PSME1 (indicated by arrows in Fig. 6E–H), and could also be encountered in AECII near more dense fibrotic regions in fNSIP lungs (Suppl. Fig. E7), whereas IPF-AECII near zones of dense fibrosis (Fig. 6I, J) or near areas of active fibrotic remodelling (Fig. 6K) indicated no or weak expression of this proteasomal subunit (indicated by arrows in Fig. 6M, N, O). In some cases, a pronounced PSME1 staining was also encountered in IPF-AECII near dense fibrotic regions (not shown), but was nevertheless generally weaker as compared to fNSIP lungs. Furthermore, PSME1 expression was absent in fibroblast foci of IPF lungs (Fig. 6O). With regard to control lung tissues, "normal" AECII indicated no significant expression of PSME1 (see arrows in Fig. 6L, P). Finally, considerable expression of PSME1 was generally observed in interstitial inflammatory cells (especially lymphocytes) of fNSIP-, IPF- and control lungs (Fig. 6M, N; Suppl. Fig. E7).

We next went on to characterize the localization of expression of peroxiredoxin 6 (PRDX6) in fNSIP-, IPF- and control lungs. Abundant PRDX6 expression was observed in AECII of thickened

**Table 4 – Proteins significantly differentially regulated in fNSIP lungs relative to IPF lung tissue: RF ≥ 1.5 for upregulation, RF ≤ 0.75 for downregulation.**

| Spot no. | Accession number (NCBI)/Protein name | Score Est´d Z (Z-score) | Seq. cov. (%) | Matched peptides | Theor. MW [kDa] | RF_ NSIP/ IPF | RF_ NSIP/ donor | RF_ IPF/ donor |
|---|---|---|---|---|---|---|---|---|
| | **Upregulated Proteins** | | | | | | | |
| **3175** | gi\|3212456: Chain A, chrystal structure of human serum albumin (ALB) | 2.39 | 36 | 24 | 68.45 | 1.607 | 2.1257 | 1.3218 |
| 2714* | gi\|494296: Chain B, Cathepsin D (CTSD) | 2.35 | 65 | 16 | 26.46 | 1.596 | 2.3507 | 1.4731 |
| 3189 | gi\|38566176: Phosphoglycerate mutase 1 (PGAM1) | 2.41 | 76 | 22 | 28.92 | 1.607 | 3.3580 | 2.0911 |
| 2904 | gi\|5453990: proteasome activator complex subunit 1 (PSME1), proteasome activator 28 subunit alpha (PA28 alpha), 11S regulator complex subunit alpha | 1.91 | 44 | 12 | 28.88 | 1.583 | 2.2898 | 1.4468 |
| 3198† | gi\|15277503: ACTB protein, actin beta | 2.21 | 38 | 16 | 40.54 | 1.759 | 5.1477 | 2.9279 |
| 3191 | gi\|4758638: peroxiredoxin 6 (PRDX6) | 2.32 | 70 | 15 | 25.13 | 1.544 | 1.5162 | 0.9823 |
| 2960 | gi\|9955007: Chain A, Thioredoxin Peroxidase B from red blood cells | 2.37 | 66 | 20 | 21.68 | 1.521 | 0.6125 | 0.4014 |
| 3075 | gi\|229752: Chain B, Alpha-Ferrous-Carbonmonoxy, Beta-Cobaltous-Deoxy-Hemoglobin (T-State) | 2.40 | 99 | 15 | 15.96 | 1.618 | 1.5674 | 0.9703 |
| 2748 | gi\|229383: cytochrome b5 fragment (CYB5A) | 1.66 | 87 | 7 | 10.01 | 1.825 | 3.5195 | 1.9309 |
| | **Downregulated proteins** | | | | | | | |
| 3072 | Mixture | | | | | 0.463 | 3.0437 | 6.5791 |
| | 1. gi\|14043271: keratin, type I cytoskeletal 19, cytokeratin-19 (KRT19) | 2.16 | 57 | 32 | 44.07 | | | |
| | 2. gi\|16552261: unnamed protein product, vimentin (VIME) | 2.34 | 33 | 14 | 47.53 | | | |

Definition of abbreviations: RF = regulation factor; Est´d Z: Z-score/Profound score: a Z-score of ≥1.65 is considered significant at the 5% level ($p < 0.05$); Seq. cov. (%) = sequence coverage in %; Theor. MW [kDa] = theoretical molecular weight in kDa.
* = Cathepsin D heavy chain identified; † = spot migrates with MW ~29 kDa in 2-DE.

alveolar septae in fNSIP lungs (indicated by arrows in Fig. 7A–B and E–F), and in AECII near zones of dense fibrosis in IPF lungs (indicated by arrows in Figs. 7C–D and G–H), as well as in "normal" AECII of control lungs (indicated by arrows in Fig. 7M-P). Additionally, robust expression of PRDX6 was observed in ciliated bronchial cells in IPF lungs (indicated by dashed arrows in Fig. 7I-K), but not in non-ciliated clara cells (indicated by CC10 staining in Fig. 7J). The same observation was made in bronchioles of fNSIP lungs (not shown) and control lungs (Fig. 7M). Fibroblastic cells of IPF lungs did not reveal pronounced expression of PRDX6, whereas some inflammatory cells in the interstitium of fNSIP-, IPF- and control lungs indicated considerable PRDX6 expression. However, differences in cellular expression of PRDX6 could not be observed in IHC, possibly due to high abundance of this enzyme in the human lung [41]. Immunoblot analysis of BALF samples for PRDX6 revealed reduced protein levels in fNSIP and IPF in comparison to HV, but PRDX6-protein contents were still higher in fNSIP when compared to IPF (Fig. 7Q and R). However, these results were not statistically significant.

Finally, we focused our research on cytokeratin-19 (KRT19), which occurred on several positions in the 2D-gel, thereby indicating different fold changes/RF-values in the comparisons IPF/fNSIP versus controls (Fig. 1A and B, Tables 2 and 4). First, one KRT19 spot appeared to be equally upregulated in fNSIP- and IPF- versus control lungs according to the DIGE analysis (Fig. 1A, Table 2). Further, KRT19 protein was identified in a protein spot containing a mixture of KRT19 and vimentin (VIME), presumably due to comigration as a result of the similar MW and pI (isoelectric point) of both proteins (indicated in Fig. 1B and Table 4). This spot appeared to be upregulated in IPF- and fNSIP- relative to control lungs, and was nevertheless twice as much downregulated in fNSIP- relative to IPF lungs according to the DIGE analysis (Table 4). We therefore investigated the localization of KRT19 expression in fNSIP-, IPF- and control lungs by IHC. KRT19 was expressed in an induced fashion in AECII of thickenend alveolar septae (Fig. 8A, E) and in AECII overlying areas of uniform dense fibrosis in fNSIP lungs (Fig. 8B, F), as well as in AECII near areas of fibrotic remodelling and bronchiolization in IPF lungs (Supplementary Fig. E8). In contrast, "normal" AECII of control lungs indicated only faint expression of KRT19 (Fig. 8C, G). In IPF/UIP lungs, KRT19 overexpression was (beside AECII) strikingly evident in bronchial structures (bronchiolar basal cells and ciliated and non-ciliated bronchial cells, see Fig. 8D) in areas of bronchiolization and honeycomb cyst formation, which are indicated by KRT5

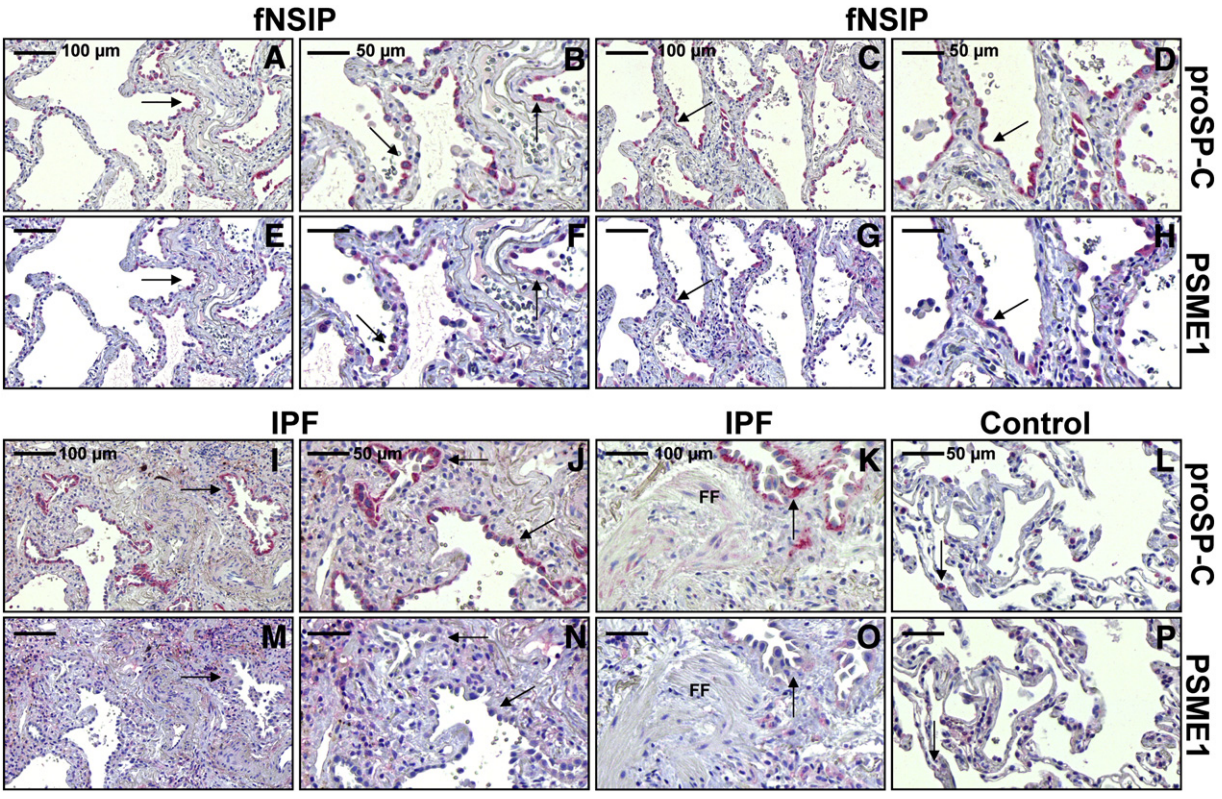


**Fig. 6 – Induction and upregulation of proteasome activator complex subunit 1 (PSME1) in type-II alveolar epithelial cells (AECII) in fibrotic NSIP lungs. Representative immunohistochemistry for proSP-C (A–D, I–K) and PSME1 (E–H, M–O) in serial sections of fNSIP- and IPF lung tissues, and for proSP-C (L) and PSME1 (P) in control lungs. (A–D, E–H) AECII in areas of thickened alveolar septae in fibrotic NSIP lungs (fNSIP; A–D) reveal robust expression of PSME1 (see arrows in E–H). (I–K, M–O) AECII near areas of dense fibrosis (I, J) and active fibrotic remodelling (K) indicate no or only sparse PSME1 expression (see arrows in M, N and O). (L, P) AECII of control lungs indicate no significant expression of PSME1 (indicated by arrows). In general, PSME1 expression is also found in some interstitial inflammatory cells in fNSIP, IPF- and control lungs (G, M–P). Original magnification of photomicrographs A, C, E, G, I, M: ×200 (bar = 100 µm); original magnification of photomicrographs B, D, F, H, J–L, N–P: ×400 (bar = 50 µm).**

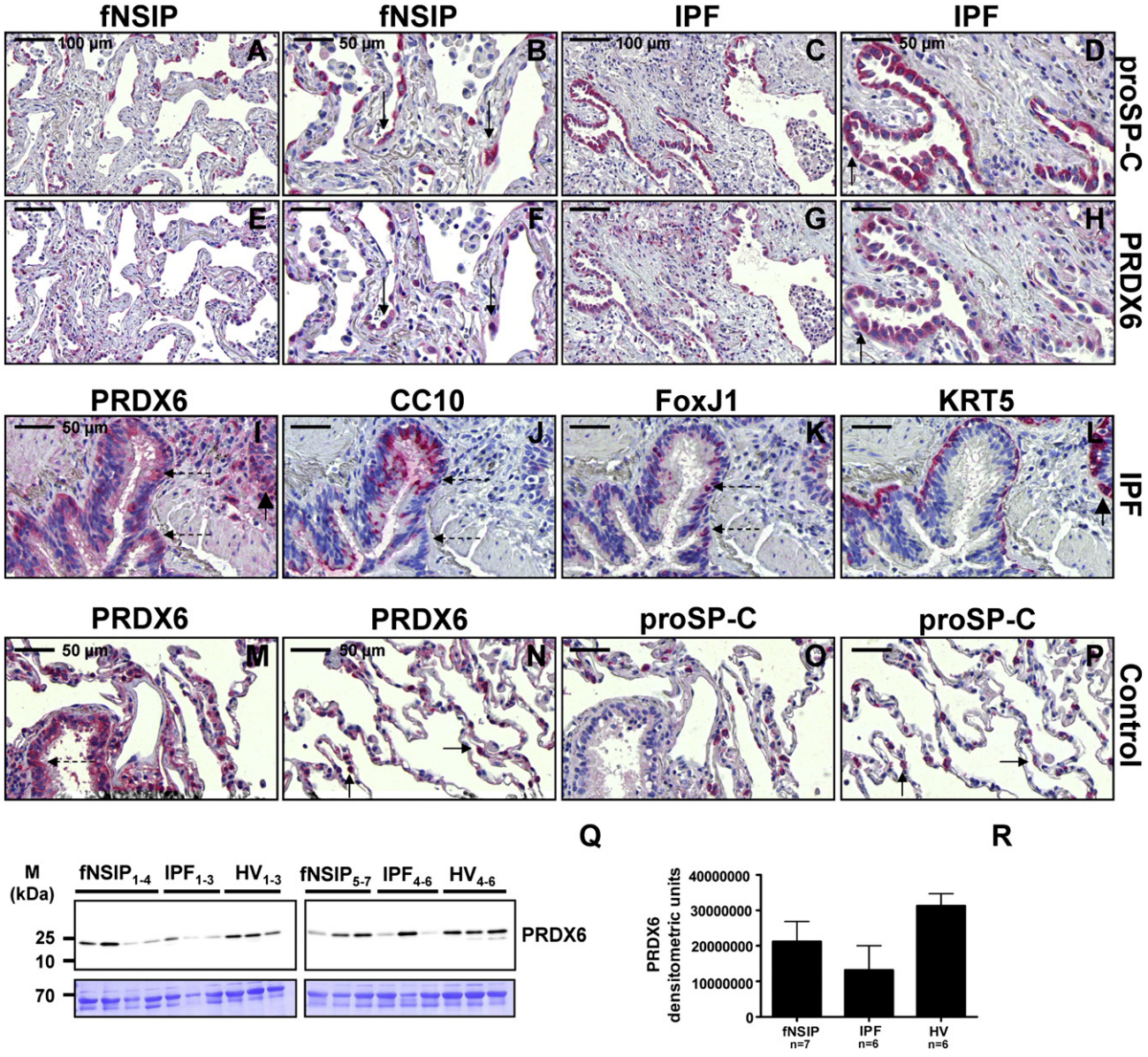


**Fig. 7 – Expression analysis of peroxiredoxin 6 (PRDX6) in lungs from patients with fibrotic NSIP and IPF in comparison to Control lungs. Representative immunohistochemistry for proSP-C (A–D), PRDX6 (E–H, I), clara cell-protein 10 [CC10] (J), FoxJ1 (K) and cytokeratin-5 [KRT5] (L) in serial sections of fNSIP- and IPF lung tissues, and for PRDX6 (M, N) and proSP-C (O, P) in control lungs. (A–D, E–H) AECII in areas of thickened alveolar septae in fibrotic NSIP lungs (fNSIP; A, B, E, F) as well as AECII near zones of dense fibrosis in IPF lungs (C, D, G, H) reveal robust expression of PRDX6 (indicated by arrows). (I–L) In IPF lungs, PRDX6 expression is also found in ciliated bronchial cells which are marked by FoxJ1-staining in a parallel section (K) and dashed arrows in Figs. I, J and K. Non-ciliated clara cells (as indicated by CC10 staining in J) don´t express PRDX6 (I and J). Moderate PRDX6 expression is also observed in some bronchiolar basal cells in IPF lungs (indicated by KRT5-staining in L and arrowheads in I and L). (M–P) In control lungs, PRDX6 is robustly expressed in AECII (indicated by arrows) and ciliated bronchial cells (indicated by dashed arrows). Original magnification of photomicrographs A, C, E, G: ×200 (bar = 100 μm); original magnification of photomicrographs B, D, F, H, I–L and M–P: ×400 (bar = 50 μm). (Q) Representative immunoblot and (R) quantitative immunoblot analysis for PRDX6 of BAL fluid from patients with sporadic fNSIP (n = 7), IPF (n = 6) and healthy volunteers (HV, n = 6). Five μg protein of cell-free BALF samples were concentrated and separated on a 15% SDS-PAGE. Coomassie staining of the blot membrane was used as a loading control. Intensity of bands was densitometrically quantified and presented as column diagram for each category (mean ± SEM).**

staining of the basal layer of bronchioles in a serial section (Fig. 8H). Immunoblot analysis of BALF samples for KRT19 revealed significantly enhanced protein contents of a ~25 kDa fragment in lavages of IPF patients, in comparison to fNSIP and HV ($p < 0.05$ vs. fNSIP; $p < 0.01$ vs. HV; Fig. 8I and J). Despite reported evidence of CYFRA (cytokeratin 19 fragment, ~37 kDa) in

human BALF of IIP patients [42,43], we could not detect CYFRA as well as full-length KRT19 (~44 kDa) in concentrated lavage samples (10 μg) obtained from our IIP patient cohort.

### 3.5. *Alveolar epithelial endoplasmic reticulum (ER) stress in fibrotic NSIP and IPF*

We observed induced expression of stress-induced genes PPIA and LAP3 in AECII of lungs from fNSIP- and IPF patients, as well as encountered induced expression of the antioxidant enzyme PRDX1 and the proteasome activator PMSE1 predominantly in the AECII of fNSIP lungs. Therefore, we finally investigated the localization of expression of typical UPR/ER stress-marker (and -sensor) proteins such as activating transcription factor 6 [ATF6, including activated p50ATF6(N)] and X-box binding protein 1 (XBP1) in fNSIP- in comparison to IPF- and control lungs. AECII near dense zones of uniform fibrosis in fNSIP lungs (Fig. 9A, B) as well as AECII in areas of dense fibrotic remodelling in IPF/UIP lungs (Fig. 9D) indicated robust induction of p50ATF6/ATF6 (Fig. 9E, F, H) and XBP1 (Fig. 9I, J, L) to same extent, in comparison to "normal" AECII of control lungs which revealed no or only sparse expression of ATF6 or XBP1 (Fig. 9M, N, O). Induced and considerable overexpression of p50ATF6/ATF6 and XBP1 was also observed in AECII in areas of thickened alveolar septae of fNSIP lungs (Fig. 9C, G, K). Alveolar macrophages of fNSIP- and IPF lungs revealed also immunostaining for ATF6 (Fig. 9E, F, H), but not for XBP1 (Fig. 9I, J, L).

## 4. Discussion

We performed a comparative proteome analysis of lung tissue from patients with fNSIP and IPF and normal control lung tissue in order to identify differentially regulated proteins in fNSIP and IPF relative to controls as well as between IPF and fNSIP itself. The latter aim was challenging, because it had been reported that gene expression profiles of IPF- and NSIP lungs were quite similar and that only few differences between the two types of

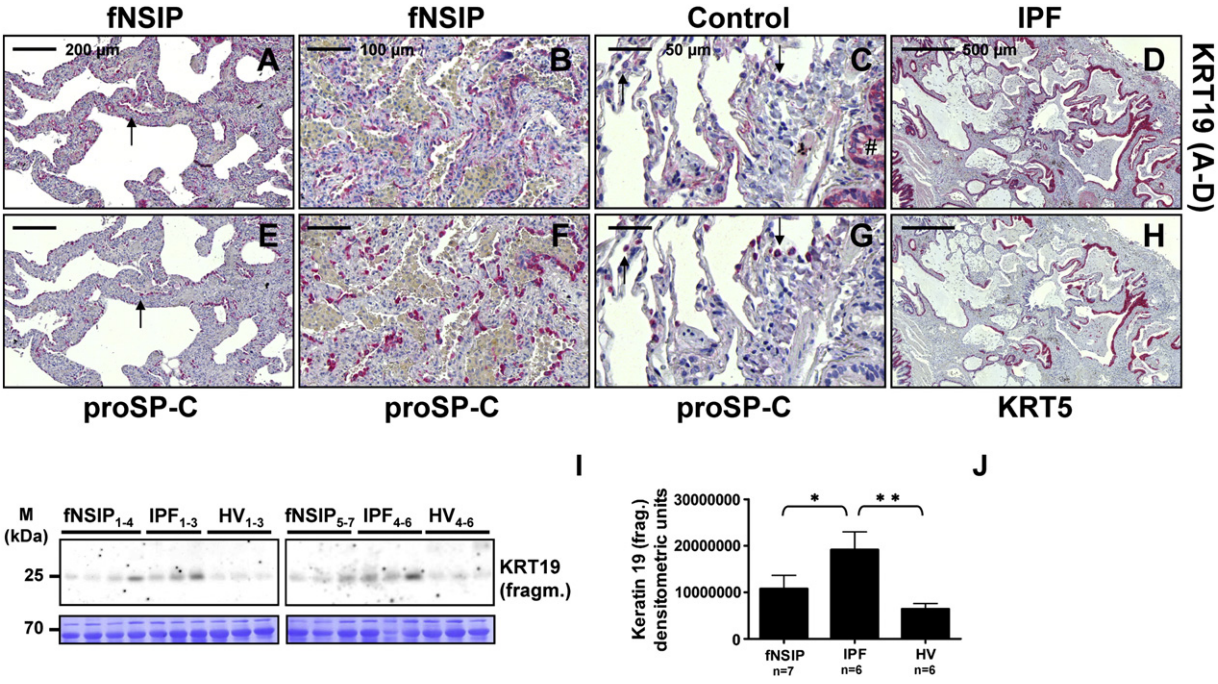


**Fig. 8 – Expression analysis of cytokeratin 19 (KRT19) in lungs from patients with fibrotic NSIP and IPF in comparison to Control lungs. Representative immunohistochemistry for cytokeratin 19 [KRT19] (A, B) and proSP-C (E, F) in fibrotic NSIP lungs (fNSIP), and for KRT19 (C) and proSP-C (G) in control lung tissues, and for KRT19 (D) and cytokeratin 5 [KRT5] (H) in IPF lungs. (A, B, E, F) In fNSIP, robust KRT19 overexpression was observed in hyperplastic AECII in areas of thickened alveolar septae (A, E) and in AECII in areas of dense uniform fibrosis (B, F). (C, G) AECII in control lungs indicate a weak basal expression of KRT19 (indicated by arrows), whereas bronchial epithelium reveal a notable constitutive KRT19 expression in normal control lungs (indicated by hashmark in C). (D, H) In IPF lungs, strong expression of KRT19 is not only observed in hyperplastic AECII (not shown), but also very dominantly in bronchiolar basal cells (indicated by KRT5 staining in H), as well as ciliated—and non-ciliated bronchial cells of abnormal bronchioles in bronchiolized areas in IPF lungs. Original magnification of photomicrographs A and E: ×100 (bar = 200 μm); original magnification of photomicrographs B and F: ×200 (bar = 100 μm); original magnification of photomicrographs C and G: ×400 (bar = 50 μm); original magnification of photomicrographs D and H: ×50 (bar = 500 μm). (I) Representative immunoblot and (J) quantitative immunoblot analysis for KRT19 of BAL fluid from patients with sporadic fNSIP (n = 7), IPF (n = 6) and healthy volunteers (HV, n = 6). 10 μg protein of cell-free BALF samples were concentrated and separated on a 10% SDS-PAGE. Coomassie staining of the blot membrane was used as a loading control. Intensity of bands was densitometrically quantified and presented as column diagram for each category (mean ± SEM). * ($p < 0.05$) for fNSIP versus HV, ** ($p < 0.01$) for IPF versus HV.**

IIP were found [10,11,31]. The challenge to analyze three different proteomes was overcome by the 2D-DIGE method, by separating and comparing the differently labelled IPF-, fNSIP- and healthy control lung proteome (IPF: Cy3, NSIP: Cy5, control: Cy2) on one and the same 2D-gel. Spot matching and quantification were improved in comparison with traditional 2D-gel-based techniques.

Our study is limited by the relatively low number of lung tissue samples for each patient category, especially for fNSIP and donor lung materials. It has, however, to be kept in mind, that both, IPF and fNSIP, are orphan diseases, with (idiopathic) fNSIP being even much less frequent as compared to IPF. To somewhat circumvent this problem, we used pooled samples of organ donor lungs as well as of explanted end-stage lungs from each patient category, in order to reduce the (everlasting) biological variation from patient to patient, and to identify robust and "real" differences. In addition, most of the relevant results/proteomic signatures were further confirmed by IHC in individual samples, and by additional analysis of BALF obtained from additional IPF- and fNSIP patients. We therefore believe that inclusion of a larger number of samples would not greatly change our findings and conclusions.

In line with previously performed transcriptional profiling of IPF and NSIP lungs [10,11,31], our results certainly indicate that both diseases are "proteomically" similar, suggesting similar pathogenetic principles and disease processes. In accordance with our previous published proteome analysis of IPF- and control lungs [33], the present data set certainly suggests that ER stress as well as a general stress-response play a crucial role in the pathogenesis of both IPF and fNSIP. Among the upregulated proteins in IPF and fNSIP were stress-induced proteins, such as leucine aminopeptidase (LAP3) and peptidylprolyl isomerase A (PPIA), the latter being also described to be involved in the UPR [44]. With its chaperone and PPIase activities, PPIA ascertains the correct folding and conformation of nascent or denaturated proteins, and also provides protection against environmental insults. LAP3 has been reported to catalyze the initial processing of antigenic proteins in the cytoplasm, which is a necessary step for antigen presentation and recognition by cytotoxic T lymphocytes (CTLs) [34]. As expected, both stress-induced genes

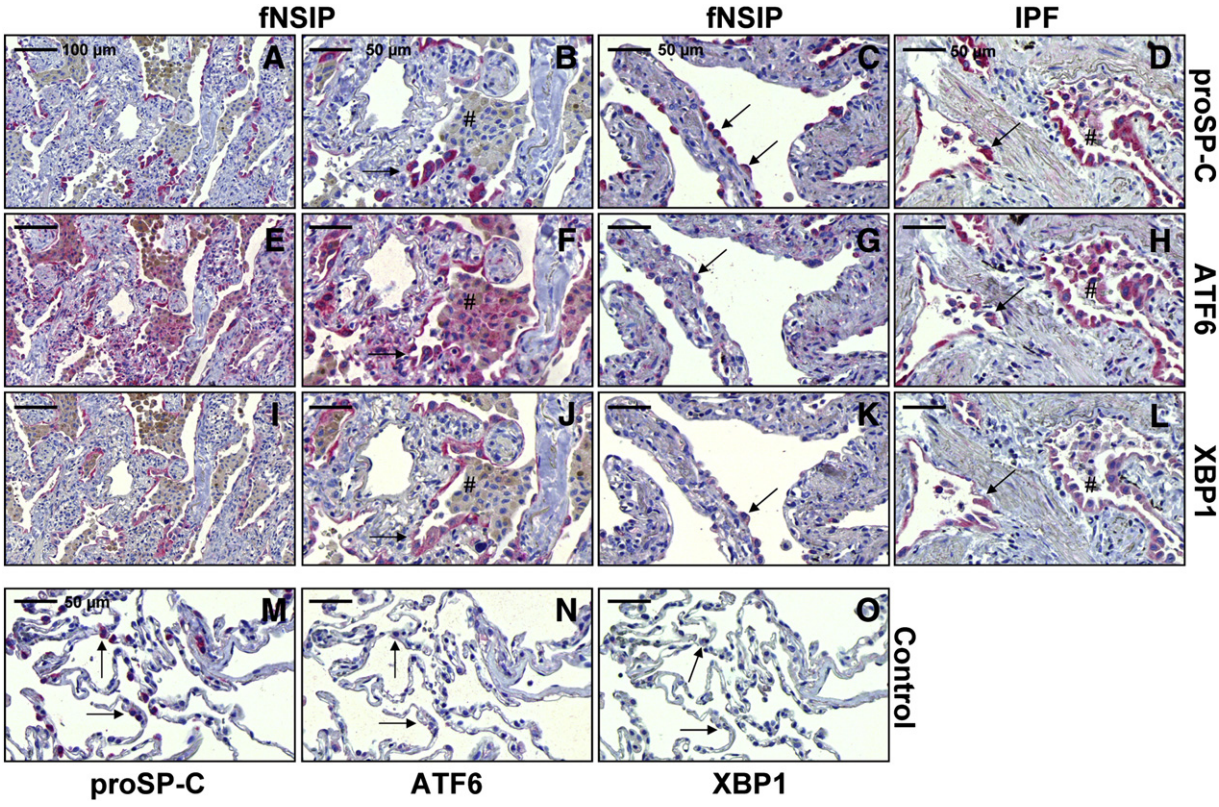


**Fig. 9 – Induction of markers for the Unfolded Protein Response (UPR) in type-II alveolar epithelial cells (AECII) in fibrotic NSIP and IPF lungs. Representative immunohistochemistry for proSP-C (A–D), activating transcription factor 6 [ATF6] (E–H) and X-box binding protein 1 [XBP1] (I–L) in serial sections of fNSIP- and IPF lung tissues, and for proSP-C (M), ATF6 (N) and XBP1 (0) in control lungs. (A–D), (E–H), (I–L) AECII in areas of dense uniform fibrosis in fibrotic NSIP lungs (fNSIP; A, B, E, F, I, J) as well as AECII in areas of active fibrotic remodelling in IPF lungs (D, H, L) reveal very strong expression of ATF6 and XBP1 to same extent (AECII are indicated by arrows). Alveolar macrophages of fNSIP and IPF lungs (indicated by hashmarks) reveal also expression of ATF6 (F and H), but not of XBP1 (J and L). Expression of ATF6 and XBP1 is also observed in AECII in areas of thickened alveolar septae in fNSIP lungs (see arrows in C, G, K). (M, N, O) In control lungs, no or only sparse expression of ATF6 and XBP1 is observed in the AECII (indicated by arrows). Original magnification of photomicrographs A, E, I: ×200 (bar = 100 µm); original magnification of photomicrographs B–D, F–H, J–L: ×400 (bar = 50 µm).**

were observed to be predominantly overexpressed in the AECII in the fibrotic lung: AECII of thickened alveolar septae and near areas of dense uniform fibrosis in fNSIP lungs as well as AECII near dense fibrotic regions in UIP/IPF lungs showed robust PPIA- or LAP3 expression, whereas "normal" AECII of control lungs indicated no or only a basal, lower expression of both enzymes (Figs. 2 and 3). Importantly, PPIA expression is not only induced by the UPR, but also induced in response to a wide variety of stressors including cancer [45]. PPIA is upregulated in many cancers [45,46], and probably functions in maintaining the conformation of oncogenic proteins. It has also been suggested that PPIA exerts in tumor cells an anti-apoptotic function by sequestering cytochrome c [47]. Upregulation of PPIA was also observed in "abnormal" bronchiolar basal cells of IPF lungs, but not in the basal layer of normal bronchioles in control lungs (Fig. 2I–N). We suggest that induced overexpression of PPIA in basal cells may be one cause for the (observed) exaggerated, proliferative character of this cell type in IPF and thus govern the process of bronchiolization in this disease.

As expected, antioxidant enzymes such as peroxiredoxin 1 (PRDX1) were observed to be upregulated in fNSIP and IPF, presumably as a response to (reported) increased oxidative stress in IIP´s [48–50]. Moreover, it has recently been shown that homozygous $Prdx1^{(-/-)}$ knockout mice are more susceptible to bleomycin-induced lung fibrosis in comparison to wild-typ mice, with marked increases in pulmonary ROS levels in diseased knockout mice, thus underscoring the crucial role of Prdx1 in protection against pulmonary fibrosis because of its antioxidant actions [51]. For validation of upregulated PRDX1 expression, we analyzed its cellular distribution in fNSIP-, IPF- and normal control lungs by IHC. Interestingly, we found PRDX1 to be mainly expressed in ciliated bronchial cells and in alveolar macrophages in fNSIP-, IPF- and control lungs (with pronounced upregulation in fNSIP- and IPF lungs vs. controls), whereas "hyperplastic" AECII in IPF- as well as "normal" AECII in control lungs did not reveal a notable expression of PRDX1 (Fig. 4A–K). Much to our surprise, we observed a prominent induction of PRDX1 in hyperplastic AECII in areas of thickened alveolar septae in some fNSIP lungs (Fig. 4L–Q, Suppl. Fig. E6I-P). Of note, "hyperplastic" AECII near areas of dense uniform fibrosis in fNSIP lungs did—similar to the AECII of UIP/IPF lungs—never reveal a significant PRDX1 expression. Taken together, the impressive finding of an AECII-localized upregulation of PRDX1 exclusively in NSIP-typical areas such as thickened alveolar septae in fNSIP lungs may represent an attempt by these AECII to adjust to the microenvironment in a manner that is advantageous to survival. According to this notion, induction of ER stress sensed by the ATF6 and IRE1/XBP1-pathways was also encountered in AECII in areas of thickened alveolar septae in fNSIP lungs (Fig. 9). Oxidative stress is known to disrupt protein folding through formation of protein carbonyls; and oxidative stress and ER stress-response are tightly interconnected through the PERK/Nrf2 pathway which induces cytoprotective and antioxidant acting genes such as peroxiredoxins in response to increased ROS levels and oxidant stress [52,53]. Furthermore, it has been already shown that Nrf2 is induced and upregulated in AECII of both NSIP- and IPF lungs, whereas "normal" AECII in controls did not indicate notable protein levels of this transcription factor [49,54]. Additionally, antioxidants have been reported to reduce ER stress and improve protein secretion in an in vitro model of protein misfolding [55]. Although purely speculative at present, the observed upregulation of PRDX1 exclusively in AECII in areas of thickened alveolar septae in fNSIP lungs could represent a protection- and survival mechanism of these AECII against oxidant-mediated cell injury and apoptosis, thereby resulting in preservation of septated alveolar structure in this histologic subtype.

Among the down-regulated proteins in fNSIP and IPF (Table 3), we identified the anti-coagulant protein annexin A5 (ANXA5), consistent with the decreased fibrinolytic activity in ILD [56]. ANXA5 is also involved in autophagosome maturation and thus directly in autophagy which is a pathway responsible for the degradation of unwanted intracellular materials. Therefore, ANXA5 is crucial for cell survival [38,57]. In line with reported oxidant-antioxidant imbalance in IIP´s [50], we observed a downregulation of some antioxidant acting enzymes, namely glutathione transferase and haptoglobin. Haptoglobin is a hemoglobin-binding acute-phase protein which possesses anti-inflammatory and antioxidative properties. Haptoglobin decreases hemoglobin-driven oxidative stress: It forms a complex with hemoglobin in order to protect the organs from damage by hemoglobin, while making the hemoglobin accessible to degradative enzymes [58,59].

Another very interesting downregulated protein in fNSIP and IPF was serum amyloid P component (SAP), a member of the pentraxin family, and which has been shown to inhibit fibrocyte differentiation *in vitro* [39,40]. In line with this observation, SAP has been recently described to reduce bleomycin-induced lung fibrosis in the mouse through attenuating bone marrow-derived mesenchymal cell accumulation and collagen synthesis [60]. Additionally, SAP has been also shown to inhibit profibrotic alternative (M2) macrophage activation and accumulation in models of pulmonary and renal fibrosis [61,62]. Another function of SAP is to scavenge nuclear material (i. e. DNA) from damaged circulating cells and to clear apoptotic and necrotic cell debris [63,64]. Interestingly, our analysis of BALF-SAP protein contents revealed significantly reduced protein levels for IPF only, as compared to healthy volunteers (HV), whereas BALF of fNSIP patients contained SAP levels similar to HV (Fig. 5)—the latter finding being in contrast to the DIGE results employing lung tissue (Table 3). On the other hand, this result is in line with reduced or no appearance of fibroblast foci in fNSIP and suggests, that BALF-SAP levels may distinguish IPF/UIP from other IIPs. Moreover, measuring of circulating levels of SAP in plasma samples has been recently undertaken in IPF patients and HV [65], indicating significantly reduced SAP concentrations in the circulation of IPF patients. Moreover, reduced SAP plasma levels predicted disease progression measured by the change in FVC (forced vital capacity) in IPF [65]. Similarly, BALF-SAP levels might also predict disease progression and severity in IPF, fNSIP, EAA and other IIP and could thus be used in the future as an additional diagnostic tool.

Finally, we identified only a few proteins that were differentially expressed between fNSIP and IPF. Among the significantly upregulated proteins in fNSIP versus IPF were the antioxidant acting proteins PRDX6 and thioredoxin peroxidase B (Table 4), suggesting that the increase of antioxidant activity is correlated to survival and better outcome and that a decline of antioxidant capacity correlates with disease progression. Another interesting, upregulated protein in fNSIP was PSME1

which has been originally described as a regulatory subunit of the proteasome implicated in antigen processing [34]. Recently, PSME1 has also been suggested to improve clearance of misfolded, oxidized proteins. Whereas overexpression of PSME1 *in vitro* was found to significantly attenuate $H_2O_2$-induced accumulation of protein carbonyls and apoptosis in cultured cardiomyocytes [66], the reverse approach, knockdown of PSME1 *in vitro*, forwarded enhanced susceptibility to oxidant cell injury [67]. Similar to conventional antioxidant enzymes such as peroxiredoxins or glutathione transferase, PSME1 is also a target of the cytoprotective antioxidant transcription factor Nrf2, and induced in response to oxidative stress [68]. Only recently, induction of proteasome activator complex subunit 1 was also shown to be involved in the removal of modified proteins during the process of differentiation [69]. Thus, the observed induction of PSME1 in AECII in areas of thickened alveolar septae in fNSIP lungs (Fig. 6) may contribute to improved cellular survival in this disease.

Peroxiredoxin 6 (PRDX6) is the isoform (out of all six mammalian peroxiredoxins) expressed at the highest level and its lung expression exceeds that for other organs [41]. PRDX6 has several properties that distinguish its peroxidase activity from other peroxiredoxins: First, it can reduce phospholipid hydroperoxides in addition to other organic hydroperoxides and $H_2O_2$. Second, PRDX6 uses GSH as an electron donor—and not thioredoxin—to reduce hydroperoxides. Third, PRDX6 has also a ($Ca^{2+}$-independent) phospholipase A2 activity which plays an important role in lung surfactant homeostasis and is responsible for degradation of internalized dipalmitoylphosphatidylcholine [41]. Transgenic mice overexpressing Prdx6 have increased defense against lung injury induced by hyperoxia, whereas $Prdx6^{(-/-)}$ knockout mice were more sensitive to the toxic effects of hyperoxia or paraquat [70,71]. Other studies with homozygous $Prdx6^{(-/-)}$ knockout mice indicated that lack of Prdx6 exaggerates lipopolysaccharide-induced acute lung injury and inflammation with increased oxidative stress [72]. Furthermore, lens epithelial cells isolated from $Prdx6^{(-/-)}$ knockout mice had enhanced expression of ER stress response genes, were sensitive to oxidative stress, and showed abnormal phenotypes with spontaneous apoptosis [73].

With regard to our DIGE data, we observed a significant upregulation of PRDX6 in fNSIP compared to IPF and controls, with no changes in PRDX6 expression between IPF and controls (Table 4). Using IHC, a very strong expression of PRDX6 was encountered in AECII of fNSIP-, IPF- and control lungs to similar extent (Fig. 7); and it could not be differentiated between PRDX6 expression in AECII of thickened alveolar septae and AECII overlying areas of dense fibrosis, presumably due to its particularly high level in lung.

A protein spot containing KRT19 and vimentin (VIME) due to comigration as a result of similar MW and pI of both proteins was the onliest significantly downregulated spot in fNSIP versus IPF, but was upregulated in both fNSIP and IPF relative to controls (Table 4). Since vimentin is a cytoskeletal protein associated with the function of fibroblasts, its reduced expression in fNSIP- versus IPF lungs was conceptional, due to generally reduced tissue fibrosis in NSIP. With regard to KRT19, we validated its downregulation via IHC. KRT19 is a specific cytoskeletal structure protein for simple-type epithelia, including bronchial and alveolar epithelial cells (BAEC). In fNSIP, KRT19 expression was robustly expressed in an induced fashion in hyperplastic AECII compared to normal AECII in control lungs, and was dominating in AECII in fNSIP lungs. In UIP/IPF lungs, KRT19 expression was certainly found in AECII, but was also particularly dominating in basal and luminal bronchiolar cells in areas of bronchiolization, including epithelial abnormalities such as squamous metaplasia lining the honeycomb-regions (Fig. 8, Suppl. Fig. E8). Thus, KRT19 upregulation in IPF versus fNSIP highlighted the phenomenon of aberrant epithelial repair in IPF such as the bronchiolization-process which is a hallmark of the UIP pattern [1,3,15,17]. In line with this, increased BALF and serum levels of cytokeratin 19 fragment (CYFRA) have been reported to reflect ongoing epithelial injury and repair in IPF [42,43]. However, we could not detect CYFRA or full-length KRT19 in concentrated lavage samples by immunoblotting. Instead, we observed significantly elevated protein levels of a ~25 kDa fragment of KRT19 in BALF of IPF patients in comparison to fNSIP and HV [Fig. 8I, J], possibly reflecting only the process of epithelial instability and apoptosis in IPF, but not extensive regeneration of epithelial cells. KRT19 has been described as a caspase-3 substrate [74,75] and is cleaved by it in response to induction of apoptosis by anisomycin [76].

Taken together, our DIGE data including validation experiments suggest that there are consistent, but only few differences between IPF and fNSIP at the proteomic level. In comparison to IPF, the proteomic signature of fNSIP was enriched for genes which are functionally associated with defense mechanisms against oxidative—and ER stress and thus antiapoptotic strategies. Importantly, this finding is in line with the reported transcriptomic signature in NSIP lungs, revealing downregulation of the proapoptotic p53 kinase HIPK2 in this entity versus IPF lungs—and thus reduced apoptosis in NSIP. With regard to normal control lungs, HIPK2 was upregulated in both NSIP and IPF [10]. Additionally, the obtained fNSIP signature of increased antioxidant capacity in alveolar epithelium is in line with previous IHC-studies reporting decreased expression of apoptotic proteins (p53, p21) in (alveolar) epithelial cells of NSIP- in comparison to IPF lungs [23,24]. We therefore conclude that the impressive finding of an AECII-localized upregulation of antioxidant acting enzymes as well as of factors involved in the removal of oxidized proteins in fNSIP lungs may represent an attempt of these AECII to survive under conditions of persistent ER- and oxidative stress (Fig. 10), thereby resulting in the maintenance of septated alveolar structure in this distinct histologic subtype.

Taken together, our data indicate that central molecular events in the pathogenesis of IPF and fNSIP are localized to the alveolar epithelium, and put forward antioxidant therapeutic approaches to inhibit detrimental oxidant-mediated reactions (which may also originate from chronic ER stress) in these fatal diseases.

### 4.1. *Correlation of proteomic changes with functional data*

With regard to SAP, we performed a linear regression analysis between SAP-BALF levels and DLCO/SB values from fNSIP- and IPF patients, and observed no significant correlation of SAP-BALF levels with DLCO/SB [Suppl. Fig. E9B]. Importantly, we observed a significant correlation of BALF-SAP with DLCO ($r^2 = 0.50$, $p = 0.0224$) when IPF patients and HV were included in the analysis [Suppl. Fig. E9C]. Further linear regression

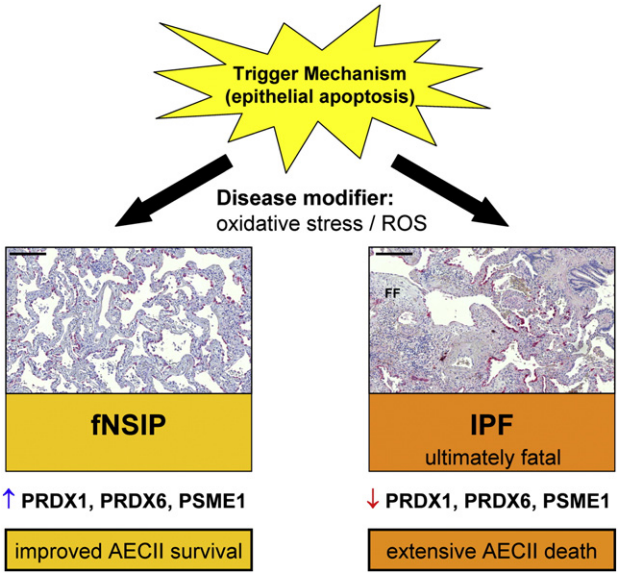


**Fig. 10 – Oxidant-mediated injury and the decline of antioxidant capacity are key in the pathogenesis of fibrotic NSIP and IPF. The scheme depicts a unifying pathomechanistic concept underlying sporadic fibrotic NSIP (fNSIP) and IPF, indicating epithelial injury as the triggering event. Oxidative stress originating from exogenous "second hits" such as inhalative noxes (smoking, air pollution) or from endogenous ER stress is disease-determinant, and triggers and results in increased AECII apoptosis and fibrosis. In fNSIP, signatures of enhanced protection mechanisms against oxidative—and ER stress in alveolar epithelium distinguish this disease from IPF, and might explain the better outcome and survival in that entity. AECII are indicated by proSP-C staining in photomicrographs, bar = 200 μm. Abbreviations: ROS = reactive oxygene species; AECII = type-II alveolar epithelial cell; FF = fibroblast foci; PRDX-1,-6 = peroxiredoxin 1 and -6, PSME1 = proteasome activator complex subunit 1.**

studies indicate that BALF levels for PRDX1 and -6 positively correlate with DLCO/SB in patients with fNSIP and IPF [Suppl. Figs. E10/E11A–C], and BALF contents for 25 kDa-KRT19 fragment displayed a significant inverse correlation with DLCO/SB in both categories [Suppl. Figs. E12A + C]. Additionally, BALF levels of PRDX6 and KRT19 fragments also correlated significantly with FVC in IPF patients [Suppl. Figs. E13A + B]. Despite the low number of patient subjects used for analyses, these preliminary correlation tests might suggest a biological relationship between SAP, PRDX1 and -6, and cleaved KRT19 fragments with the severity of lung disease in IPF and/or fNSIP.

Hence, these correlation studies offer "antioxidant" (PRDX1 and -6) or "antifibrotic" (SAP) signatures as novel biomarkers to monitor disease progression and severity in different IIPs. Future research should focus on confirming these findings and suggestions in BALF and serum in a bigger cohort of IPF- and fNSIP patients, and if this panel of proteins may be used to differentiate IPF from NSIP (and also from other IIPs), and to indicate prognosis.

## 5. Concluding remarks

In conclusion, we demonstrated for the first time a comparative proteome analysis of subpleural lung tissue from patients with sporadic IPF and fNSIP, with explanted donor lungs serving as controls. We observed that the histologically different presentations of UIP/IPF and fNSIP were proteomically similar and that only few protein expression changes exist between IPF and fNSIP. Our data suggest that ER stress and a general stress–response as well as the decline of antioxidant capacity in alveolar epithelium are key in the pathogenesis of IPF and fNSIP. Finally, we conclude that signatures of enhanced protection mechanisms against oxidative—and ER stress distinguish fNSIP from IPF, and may explain the better outcome and survival in patients with fNSIP in comparison to IPF patients (Fig. 10). These changes seem to be correlated with disease severity.

Supplementary data to this article can be found online at http://dx.doi.org/10.1016/j.jprot.2013.04.033.

## Competing interests

The authors declare that they have no competing interests.

## Acknowledgment

We thank Dr. Franka Garcia Prado (TOPLAB GmbH) for her valuable help and discussion, and we thank the technicians Silke Händel, Stefanie Hezel and Leonie Steinbach for scanning of numerous immunostained lung tissue sections.

This work has been funded by grants from the German Centre for Lung Research (DZL) and from the Bundesministerium für Bildung und Forschung ("German Network for Diffuse Parenchymal Lung Diseases", GOLDnet), as well as from the European Community's Seventh Framework Programme (FP7/2007-2013) under grant agreement no. HEALTH-F2-2007-202224 eurIPFnet.

## REFERENCES

[1] American Thoracic Society/European Respiratory Society International Multidisciplinary Consensus Classification of the Idiopathic Interstitial Pneumonias. This joint statement of the American Thoracic Society (ATS), and the European Respiratory Society (ERS) was adopted by the ATS board of directors, June 2001 and by the ERS Executive Committee, June 2001. Am J Respir Crit Care Med 2002;165:277–304.

[2] Travis WD, Hunninghake G, King Jr TE, Lynch DA, Colby TV, Galvin JR, et al. Idiopathic nonspecific interstitial pneumonia: report of an American Thoracic Society project. Am J Respir Crit Care Med 2008;177:1338–47.

[3] American Thoracic Society. Idiopathic pulmonary fibrosis: diagnosis and treatment. International consensus statement. American Thoracic Society (ATS), and the European Respiratory Society (ERS). Am J Respir Crit Care Med 2000;161:646–64.

[4] Raghu G, Collard HR, Egan JJ, Martinez FJ, Behr J, Brown KK, et al. An official ATS/ERS/JRS/ALAT statement: idiopathic pulmonary fibrosis: evidence-based guidelines for diagnosis and management. Am J Respir Crit Care Med 2011;183:788–824.

[5] Leslie KO. Historical perspective: a pathologic approach to the classification of idiopathic interstitial pneumonias. Chest 2005;128:513S–9S.
[6] du Bois R, King Jr TE. Challenges in pulmonary fibrosis—5: the NSIP/UIP debate. Thorax 2007;62:1008–12.
[7] Glaspole I, Goh NS. Differentiating between IPF and NSIP. Chron Respir Dis 2010;7:187–95.
[8] Flaherty KR, Martinez FJ. Nonspecific interstitial pneumonia. Semin Respir Crit Care Med 2006;27:652–8.
[9] Park JH, Kim DS, Park IN, Jang SJ, Kitaichi M, Nicholson AG, et al. Prognosis of fibrotic interstitial pneumonia: idiopathic versus collagen vascular disease-related subtypes. Am J Respir Crit Care Med 2007;175:705–11.
[10] Yang IV, Burch LH, Steele MP, Savov JD, Hollingsworth JW, McElvania-Tekippe E, et al. Gene expression profiling of familial and sporadic interstitial pneumonia. Am J Respir Crit Care Med 2007;175:45–54.
[11] Rosas IO, Kaminski N. When it comes to genes—IPF or NSIP, familial or sporadic—they're all the same. Am J Respir Crit Care Med 2007;175:5–6.
[12] Noble PW, Albera C, Bradford WZ, Costabel U, Glassberg MK, Kardatzke D, et al. Pirfenidone in patients with idiopathic pulmonary fibrosis (CAPACITY): two randomised trials. Lancet 2011;377:1760–9.
[13] Raghu G, Anstrom KJ, King Jr TE, Lasky JA, Martinez FJ. Prednisone, azathioprine, and N-acetylcysteine for pulmonary fibrosis. N Engl J Med 2012;366:1968–77.
[14] Selman M, Pardo A. Idiopathic pulmonary fibrosis: misunderstandings between epithelial cells and fibroblasts? Sarcoidosis Vasc Diffuse Lung Dis 2004;21:165–72.
[15] Selman M, Pardo A. Role of epithelial cells in idiopathic pulmonary fibrosis: from innocent targets to serial killers. Proc Am Thorac Soc 2006;3:364–72.
[16] King Jr TE, Pardo A, Selman M. Idiopathic pulmonary fibrosis. Lancet 2011;378:1949–61.
[17] Plantier L, Crestani B, Wert SE, Dehoux M, Zweytick B, Guenther A, et al. Ectopic respiratory epithelial cell differentiation in bronchiolised distal airspaces in idiopathic pulmonary fibrosis. Thorax 2011;66:651–7.
[18] Myers JL, Katzenstein AL. Epithelial necrosis and alveolar collapse in the pathogenesis of usual interstitial pneumonia. Chest 1988;94:1309–11.
[19] Kuwano K, Kunitake R, Kawasaki M, Nomoto Y, Hagimoto N, Nakanishi Y, et al. P21Waf1/Cip1/Sdi1 and p53 expression in association with DNA strand breaks in idiopathic pulmonary fibrosis. Am J Respir Crit Care Med 1996;154:477–83.
[20] Uhal BD, Joshi I, Hughes WF, Ramos C, Pardo A, Selman M. Alveolar epithelial cell death adjacent to underlying myofibroblasts in advanced fibrotic human lung. Am J Physiol 1998;275:L1192–9.
[21] Barbas-Filho JV, Ferreira MA, Sesso A, Kairalla RA, Carvalho CR, Capelozzi VL. Evidence of type II pneumocyte apoptosis in the pathogenesis of idiopathic pulmonary fibrosis (IFP)/usual interstitial pneumonia (UIP). J Clin Pathol 2001;54:132–8.
[22] Plataki M, Koutsopoulos AV, Darivianaki K, Delides G, Siafakas NM, Bouros D. Expression of apoptotic and antiapoptotic markers in epithelial cells in idiopathic pulmonary fibrosis. Chest 2005;127:266–74.
[23] Nakashima N, Kuwano K, Maeyama T, Hagimoto N, Yoshimi M, Hamada N, et al. The p53-Mdm2 association in epithelial cells in idiopathic pulmonary fibrosis and non-specific interstitial pneumonia. J Clin Pathol 2005;58:583–9.
[24] Jinta T, Miyazaki Y, Kishi M, Akashi T, Takemura T, Inase N, et al. The pathogenesis of chronic hypersensitivity pneumonitis in common with idiopathic pulmonary fibrosis: expression of apoptotic markers. Am J Clin Pathol 2010;134:613–20.
[25] Nogee LM, Dunbar III AE, Wert SE, Askin F, Hamvas A, Whitsett JA. A mutation in the surfactant protein C gene associated with familial interstitial lung disease. N Engl J Med 2001;344:573–9.
[26] Thomas AQ, Lane K, Phillips III J, Prince M, Markin C, Speer M, et al. Heterozygosity for a surfactant protein C gene mutation associated with usual interstitial pneumonitis and cellular nonspecific interstitial pneumonitis in one kindred. Am J Respir Crit Care Med 2002;165:1322–8.
[27] Mulugeta S, Nguyen V, Russo SJ, Muniswamy M, Beers MF. A surfactant protein C precursor protein BRICHOS domain mutation causes endoplasmic reticulum stress, proteasome dysfunction, and caspase 3 activation. Am J Respir Cell Mol Biol 2005;32:521–30.
[28] Korfei M, Ruppert C, Mahavadi P, Henneke I, Markart P, Koch M, et al. Epithelial endoplasmic reticulum stress and apoptosis in sporadic idiopathic pulmonary fibrosis. Am J Respir Crit Care Med 2008;178:838–46.
[29] Lawson WE, Crossno PF, Polosukhin VV, Roldan J, Cheng DS, Lane KB, et al. Endoplasmic reticulum stress in alveolar epithelial cells is prominent in IPF: association with altered surfactant protein processing and herpesvirus infection. Am J Physiol Lung Cell Mol Physiol 2008;294:L1119–26.
[30] Korfei M, Ruppert C, Mahavadi P, Koch M, Markart P, Witt H, et al. Abnormal accumulation of unprocessed surfactant protein (SP)-B and activation of the ER stress pathway in patients with idiopathic pulmonary fibrosis (IPF) and non-specific interstitial pneumonia (NSIP). Am J Respir Crit Care Med 2007;175:A735.
[31] Selman M, Pardo A, Barrera L, Estrada A, Watson SR, Wilson K, et al. Gene expression profiles distinguish idiopathic pulmonary fibrosis from hypersensitivity pneumonitis. Am J Respir Crit Care Med 2006;173:188–98.
[32] Gunther A, Siebert C, Schmidt R, Ziegler S, Grimminger F, Yabut M, et al. Surfactant alterations in severe pneumonia, acute respiratory distress syndrome, and cardiogenic lung edema. Am J Respir Crit Care Med 1996;153:176–84.
[33] Korfei M, Schmitt S, Ruppert C, Henneke I, Markart P, Loeh B, et al. Comparative proteomic analysis of lung tissue from patients with idiopathic pulmonary fibrosis (IPF) and lung transplant donor lungs. J Proteome Res 2011;10:2185–205.
[34] York IA, Goldberg AL, Mo XY, Rock KL. Proteolysis and class I major histocompatibility complex antigen presentation. Immunol Rev 1999;172:49–66.
[35] Rottoli P, Magi B, Perari MG, Liberatori S, Nikiforakis N, Bargagli E, et al. Cytokine profile and proteome analysis in bronchoalveolar lavage of patients with sarcoidosis, pulmonary fibrosis associated with systemic sclerosis and idiopathic pulmonary fibrosis. Proteomics 2005;5:1423–30.
[36] Landi C, Bargagli E, Bianchi L, Gagliardi A, Carleo A, Bennet D, et al. Towards a functional proteomics approach to the comprehension of idiopathic pulmonary fibrosis, sarcoidosis, systemic sclerosis and pulmonary Langerhans cell histiocytosis. J Proteomics 2013;83:60–75.
[37] Kinnula VL, Lehtonen S, Kaarteenaho-Wiik R, Lakari E, Paakko P, Kang SW, et al. Cell specific expression of peroxiredoxins in human lung and pulmonary sarcoidosis. Thorax 2002;57:157–64.
[38] Ghislat G, Knecht E. New Ca(2+)-dependent regulators of autophagosome maturation. Commun Integr Biol 2012;5:308–11.
[39] Pilling D, Buckley CD, Salmon M, Gomer RH. Inhibition of fibrocyte differentiation by serum amyloid P. J Immunol 2003;171:5537–46.
[40] Pilling D, Tucker NM, Gomer RH. Aggregated IgG inhibits the differentiation of human fibrocytes. J Leukoc Biol 2006;79:1242–51.
[41] Schremmer B, Manevich Y, Feinstein SI, Fisher AB. Peroxiredoxins in the lung with emphasis on peroxiredoxin VI. Subcell Biochem 2007;44:317–44.

[42] Dobashi N, Fujita J, Ohtsuki Y, Yamadori I, Yoshinouchi T, Kamei T, et al. Elevated serum and BAL cytokeratin 19 fragment in pulmonary fibrosis and acute interstitial pneumonia. Eur Respir J 1999;14:574–8.
[43] Inage M, Nakamura H, Kato S, Saito H, Abe S, Hino T, et al. Levels of cytokeratin 19 fragments in bronchoalveolar lavage fluid correlate to the intensity of neutrophil and eosinophil-alveolitis in patients with idiopathic pulmonary fibrosis. Respir Med 2000;94:155–60.
[44] Ostergaard L, Simonsen U, Eskildsen-Helmond Y, Vorum H, Uldbjerg N, Honore B, et al. Proteomics reveals lowering oxygen alters cytoskeletal and endoplasmatic stress proteins in human endothelial cells. Proteomics 2009;9:4457–67.
[45] Lee J. Role of cyclophilin a during oncogenesis. Arch Pharm Res 2010;33:181–7.
[46] Yang H, Chen J, Yang J, Qiao S, Zhao S, Yu L. Cyclophilin A is upregulated in small cell lung cancer and activates ERK1/2 signal. Biochem Biophys Res Commun 2007;361: 763–7.
[47] Bonfils C, Bec N, Larroque C, Del Rio M, Gongora C, Pugniere M, et al. Cyclophilin A as negative regulator of apoptosis by sequestering cytochrome c. Biochem Biophys Res Commun 2010;393:325–30.
[48] Kuwano K, Nakashima N, Inoshima I, Hagimoto N, Fujita M, Yoshimi M, et al. Oxidative stress in lung epithelial cells from patients with idiopathic interstitial pneumonias. Eur Respir J 2003;21:232–40.
[49] Markart P, Luboeinski T, Korfei M, Schmidt R, Wygrecka M, Mahavadi P, et al. Alveolar oxidative stress is associated with elevated levels of nonenzymatic low-molecular-weight antioxidants in patients with different forms of chronic fibrosing interstitial lung diseases. Antioxid Redox Signal 2009;11:227–40.
[50] Kinnula VL, Myllarniemi M. Oxidant-antioxidant imbalance as a potential contributor to the progression of human pulmonary fibrosis. Antioxid Redox Signal 2008;10:727–38.
[51] Kikuchi N, Ishii Y, Morishima Y, Yageta Y, Haraguchi N, Yamadori T, et al. Aggravation of bleomycin-induced pulmonary inflammation and fibrosis in mice lacking peroxiredoxin I. Am J Respir Cell Mol Biol 2011;45:600–9.
[52] Cullinan SB, Diehl JA. Coordination of ER and oxidative stress signaling: the PERK/Nrf2 signaling pathway. Int J Biochem Cell Biol 2006;38:317–32.
[53] Niture SK, Kaspar JW, Shen J, Jaiswal AK. Nrf2 signaling and cell survival. Toxicol Appl Pharmacol 2010;244:37–42.
[54] Mazur W, Lindholm P, Vuorinen K, Myllarniemi M, Salmenkivi K, Kinnula VL. Cell-specific elevation of NRF2 and sulfiredoxin-1 as markers of oxidative stress in the lungs of idiopathic pulmonary fibrosis and non-specific interstitial pneumonia. APMIS 2010;118:703–12.
[55] Malhotra JD, Miao H, Zhang K, Wolfson A, Pennathur S, Pipe SW, et al. Antioxidants reduce endoplasmic reticulum stress and improve protein secretion. PNAS 2008;105:18525–30.
[56] Chambers RC. Procoagulant signalling mechanisms in lung inflammation and fibrosis: novel opportunities for pharmacological intervention? Br J Pharmacol 2008;153(Suppl. 1): S367–78.
[57] Ghislat G, Aguado C, Knecht E. Annexin A5 stimulates autophagy and inhibits endocytosis. J Cell Sci 2012;125: 92–107.
[58] Ratanasopa K, Chakane S, Ilyas M, Nantasenamat C, Bulow L. Trapping of human hemoglobin by haptoglobin: molecular mechanisms and clinical applications. Antioxid Redox Signal 2013;18:2364–74.
[59] Alayash AI, Andersen CB, Moestrup SK, Bulow L. Haptoglobin: the hemoglobin detoxifier in plasma. Trends Biotechnol 2013;31:2–3.
[60] Pilling D, Roife D, Wang M, Ronkainen SD, Crawford JR, Travis EL, et al. Reduction of bleomycin-induced pulmonary fibrosis by serum amyloid P. J Immunol 2007;179:4035–44.
[61] Castano AP, Lin SL, Surowy T, Nowlin BT, Turlapati SA, Patel T, et al. Serum amyloid P inhibits fibrosis through Fc gamma R-dependent monocyte-macrophage regulation in vivo. Sci Transl Med 2009;1:5ra13.
[62] Murray LA, Rosada R, Moreira AP, Joshi A, Kramer MS, Hesson DP, et al. Serum amyloid P therapeutically attenuates murine bleomycin-induced pulmonary fibrosis via its effects on macrophages. PLoS One 2010;5:e9683.
[63] Familian A, Zwart B, Huisman HG, Rensink I, Roem D, Hordijk PL, et al. Chromatin-independent binding of serum amyloid P component to apoptotic cells. J Immunol 2001;167:647–54.
[64] Lu J, Marnell LL, Marjon KD, Mold C, Du Clos TW, Sun PD. Structural recognition and functional activation of FcgammaR by innate pentraxins. Nature 2008;456:989–92.
[65] Murray LA, Chen Q, Kramer MS, Hesson DP, Argentieri RL, Peng X, et al. TGF-beta driven lung fibrosis is macrophage dependent and blocked by serum amyloid P. Int J Biochem Cell Biol 2011;43:154–62.
[66] Li J, Powell SR, Wang X. Enhancement of proteasome function by PA28α overexpression protects against oxidative stress. FASEB J 2011;25:883–93.
[67] Pickering AM, Koop AL, Teoh CY, Ermak G, Grune T, Davies KJ. The immunoproteasome, the 20S proteasome and the PA28alphabeta proteasome regulator are oxidative-stress-adaptive proteolytic complexes. Biochem J 2010;432:585–94.
[68] Pickering AM, Linder RA, Zhang H, Forman HJ, Davies KJ. Nrf2-dependent induction of proteasome and Pa28alphabeta regulator are required for adaptation to oxidative stress. J Biol Chem 2012;287:10021–31.
[69] Hernebring M, Fredriksson A, Liljevald M, Cvijovic M, Norrman K, Wiseman J, et al. Removal of damaged proteins during ES cell fate specification requires the proteasome activator PA28. Sci Rep 2013;3:1381.
[70] Wang Y, Phelan SA, Manevich Y, Feinstein SI, Fisher AB. Transgenic mice overexpressing peroxiredoxin 6 show increased resistance to lung injury in hyperoxia. Am J Respir Cell Mol Biol 2006;34:481–6.
[71] Manevich Y, Fisher AB. Peroxiredoxin 6, a 1-Cys peroxiredoxin, functions in antioxidant defense and lung phospholipid metabolism. Free Radic Biol Med 2005;38:1422–32.
[72] Yang D, Song Y, Wang X, Sun J, Ben Y, An X, et al. Deletion of peroxiredoxin 6 potentiates lipopolysaccharide-induced acute lung injury in mice. Crit Care Med 2011;39:756–64.
[73] Fatma N, Singh P, Chhunchha B, Kubo E, Shinohara T, Bhargavan B, et al. Deficiency of Prdx6 in lens epithelial cells induces ER stress response-mediated impaired homeostasis and apoptosis. Am J Physiol Cell Physiol 2011;301:C954–67.
[74] Sheard MA, Vojtesek B, Simickova M, Valik D. Release of cytokeratin-18 and -19 fragments (TPS and CYFRA 21–1) into the extracellular space during apoptosis. J Cell Biochem 2002;85:670–7.
[75] Gassler N, Herr I, Keith M, Autschbach F, Schmitz-Winnenthal H, Ulrich A, et al. Wnt-signaling and apoptosis after neoadjuvant short-term radiotherapy for rectal cancer. Int J Oncol 2004;25:1543–9.
[76] Ku NO, Liao J, Omary MB. Apoptosis generates stable fragments of human type I keratins. J Biol Chem 1997;272:33197–203.